Electronic Supplementary Information

Axial ligand induced high electrocatalytic hydrogen evolution activity of molecular cobaloximes in homo- and heterogeneous medium

Jitendra Kumar Yadav,[a] Baghendra Singh,[b] Anjali Mishra[a], Sarvesh Kumar Pal,[a] Nanhai Singh,[a] Prem Lama,[c*] Arindam Indra[b*] and Kamlesh Kumar[a*]

[a]Department of Chemistry, Institute of Science, Banaras Hindu University, Varanasi 221005, India.

[b]Department of Chemistry, Indian Institute of Technology (BHU), Varanasi, UP-221005, India.

[c]CSIR Indian Institute of Petroleum, Light Stock Processing Division, Mohkampur, Dehradun 248005, Uttarakhand, India.

*Corresponding authors:

E-mail: *kamlesh.kumar@bhu.ac.in (Kamlesh Kumar),*

arindam.chy@iitbhu.ac.in (Arindam Indra),

prem.lama@iip.res.in (Prem Lama)

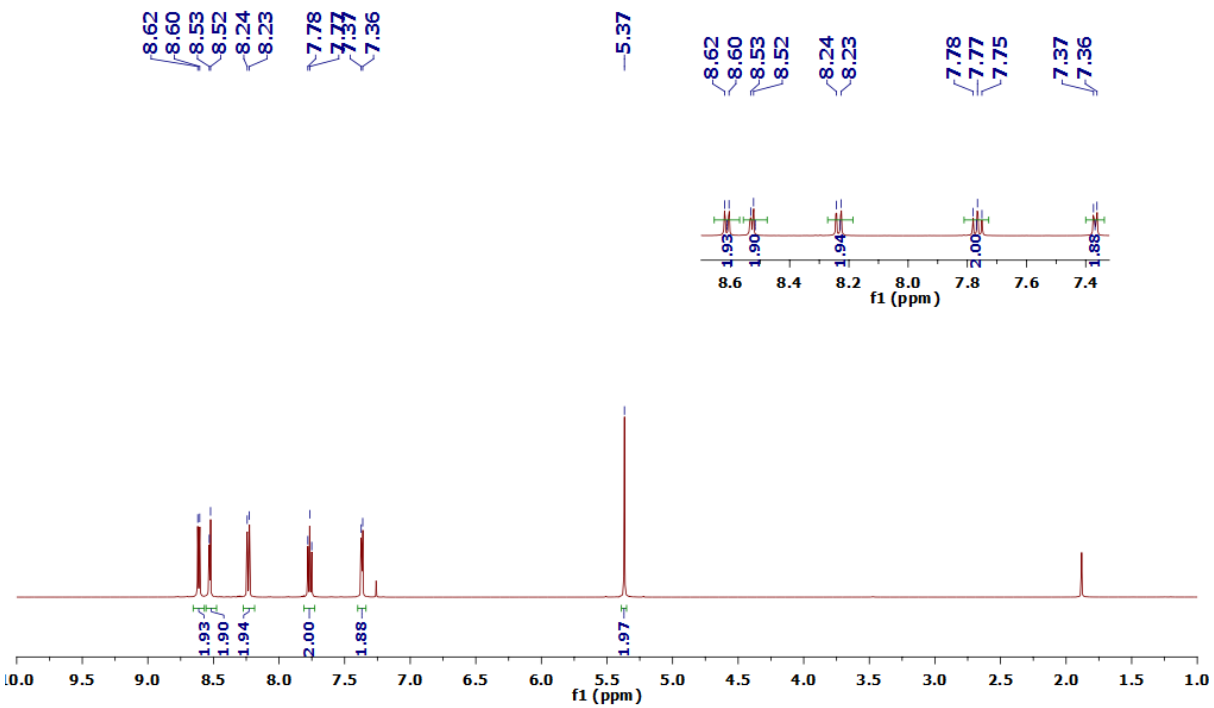

Figure S1: ^{1}H NMR spectrum (500 MHz, $CDCl_3$) of **L_1**

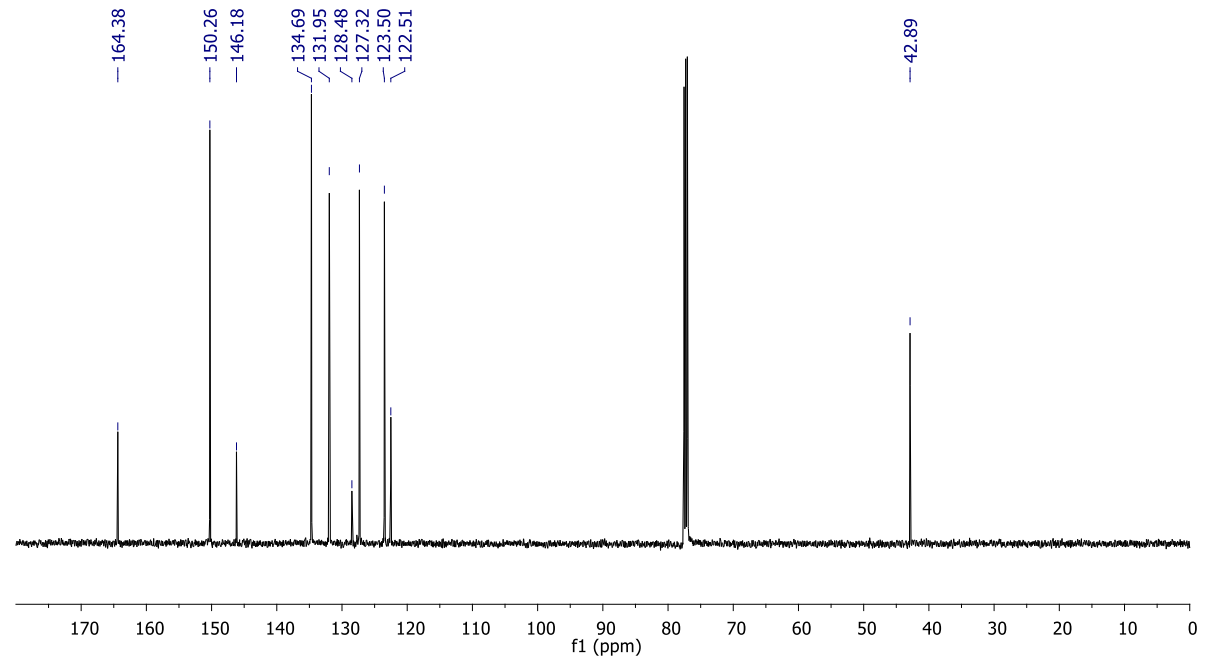

Figure S2: $^{13}C\{^{1}H\}$ NMR spectrum (125 MHz, $CDCl_3$) of **L_1**

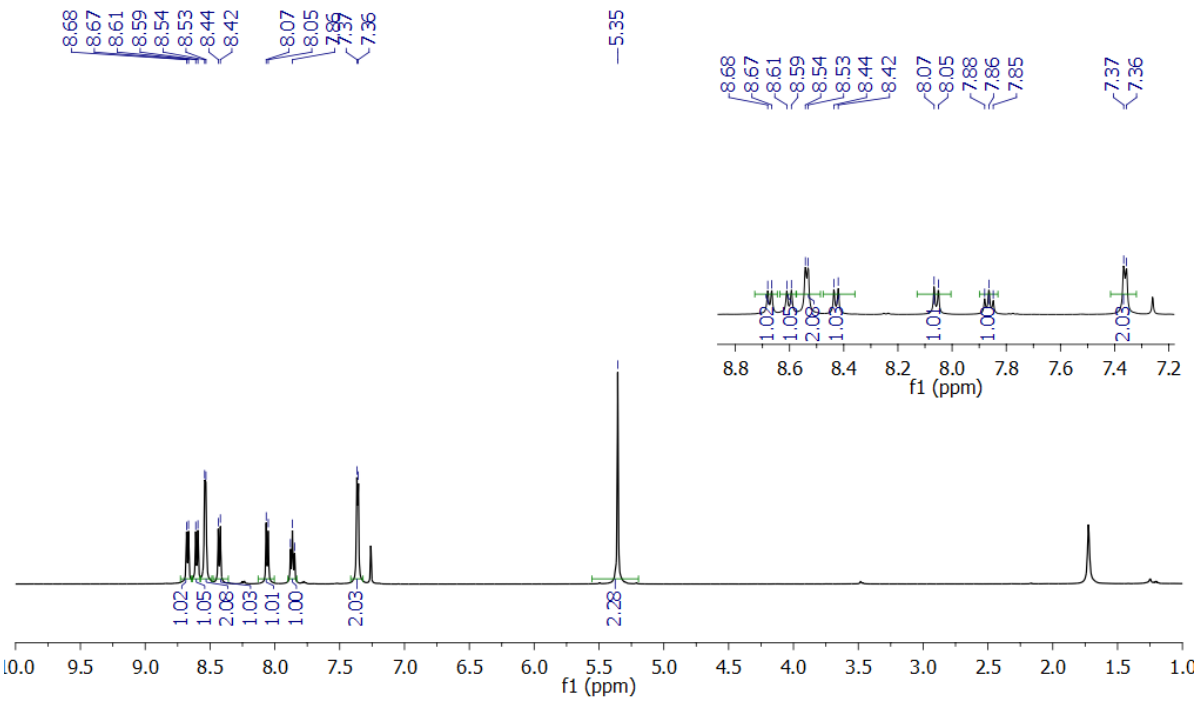

Figure S3: ^{1}H NMR spectrum (500 MHz, $CDCl_3$) of **L₂**

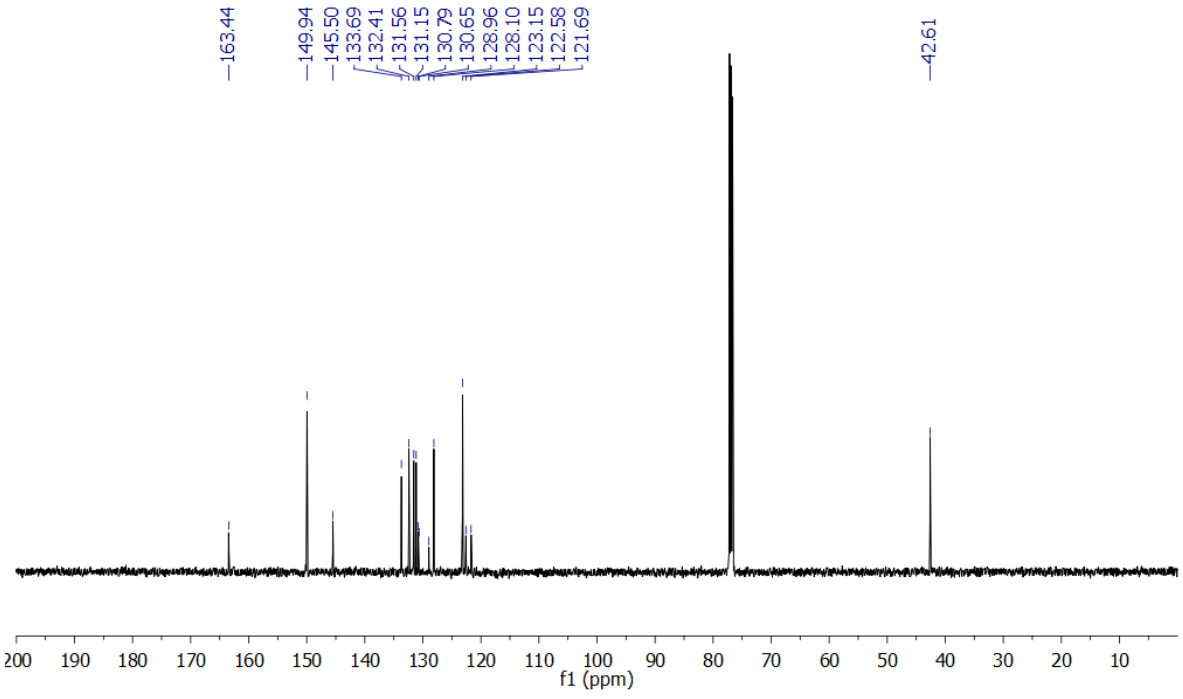

Figure S4: $^{13}C\{^{1}H\}$ NMR spectrum (125 MHz, $CDCl_3$) of **L₂**

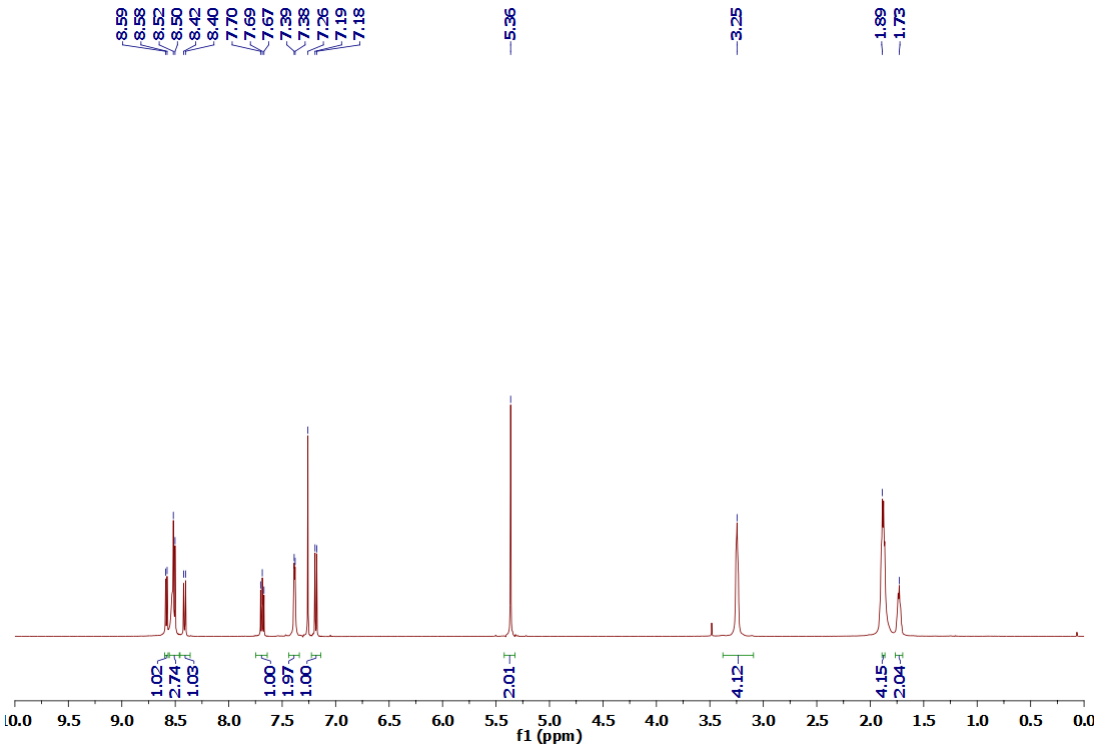

Figure S5: ^{1}H NMR spectrum (500 MHz, $CDCl_3$) of **L_3**

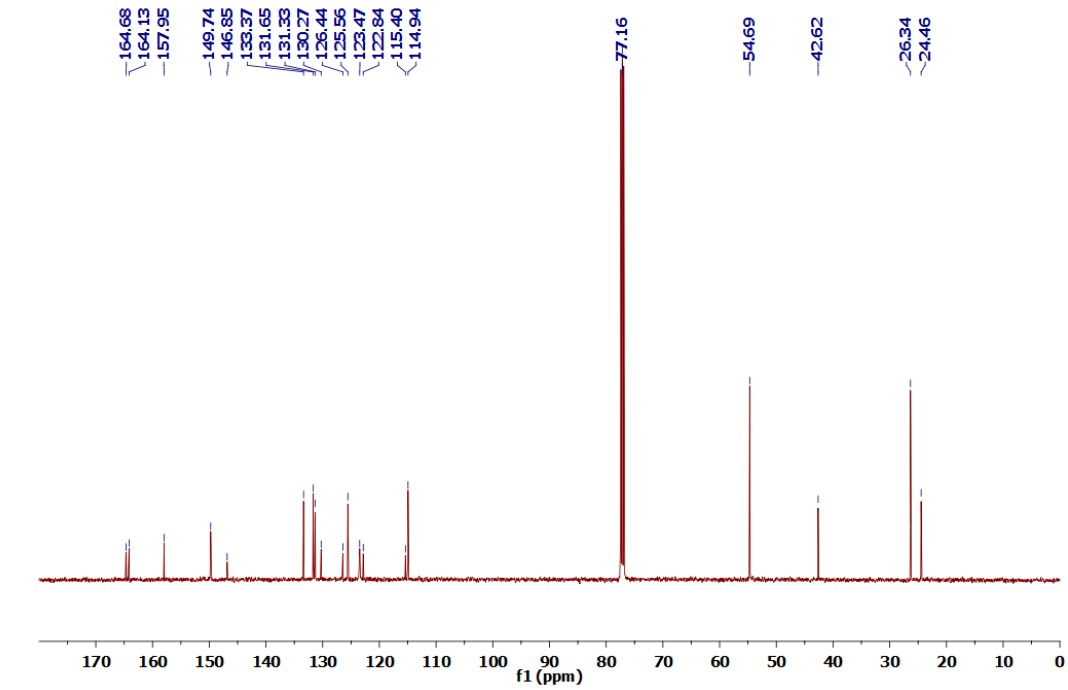

Figure S6: $^{13}C\{^{1}H\}$ NMR spectrum (125 MHz, $CDCl_3$) of **L_3**

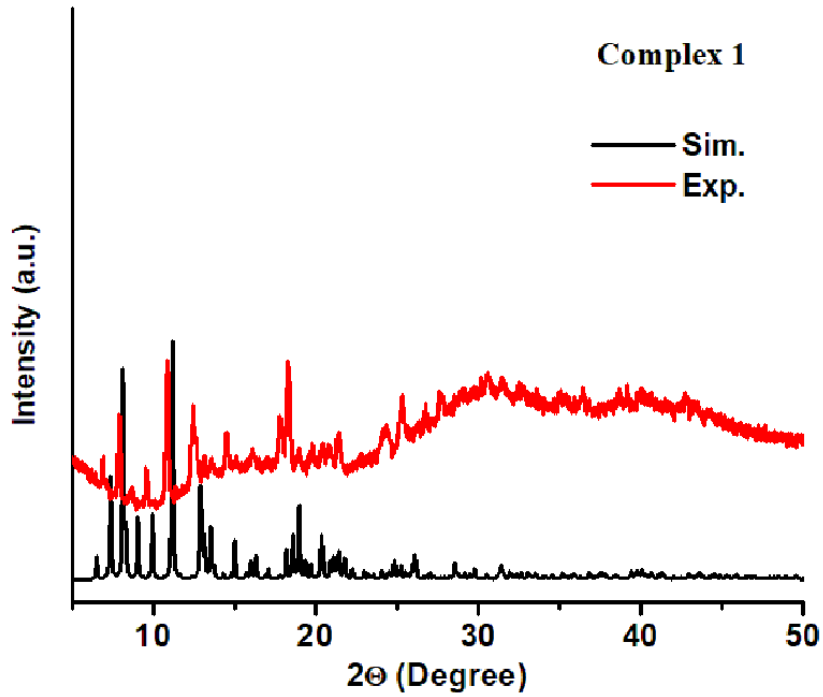

Figure S7: Simulated and experimental PXRD patterns of complex $[ClCo(dpgH)_2(L_1)]$ **(1)**

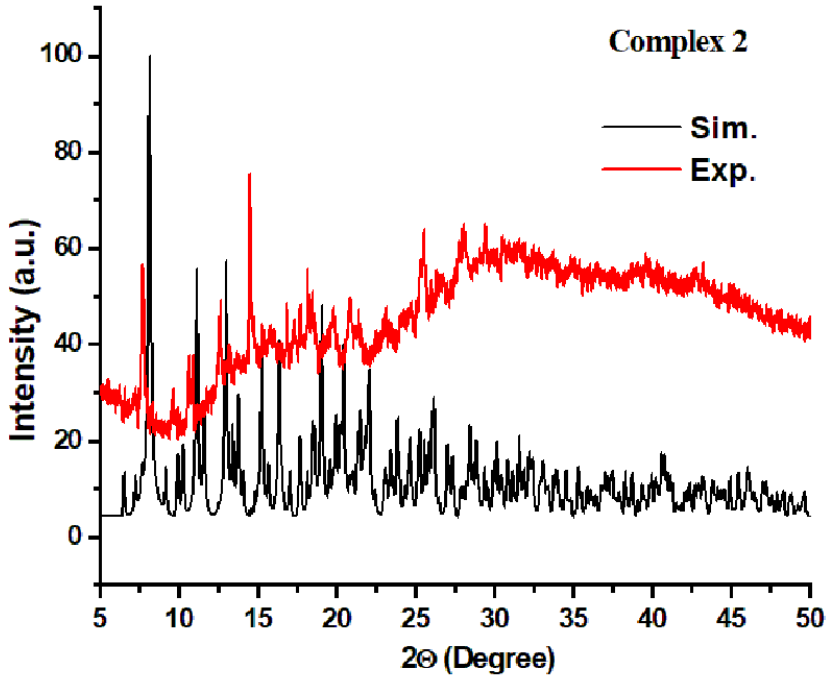

Figure S8: Simulated and experimental PXRD patterns of complex $[ClCo(dpgH)_2(L_2)]$ **(2)**

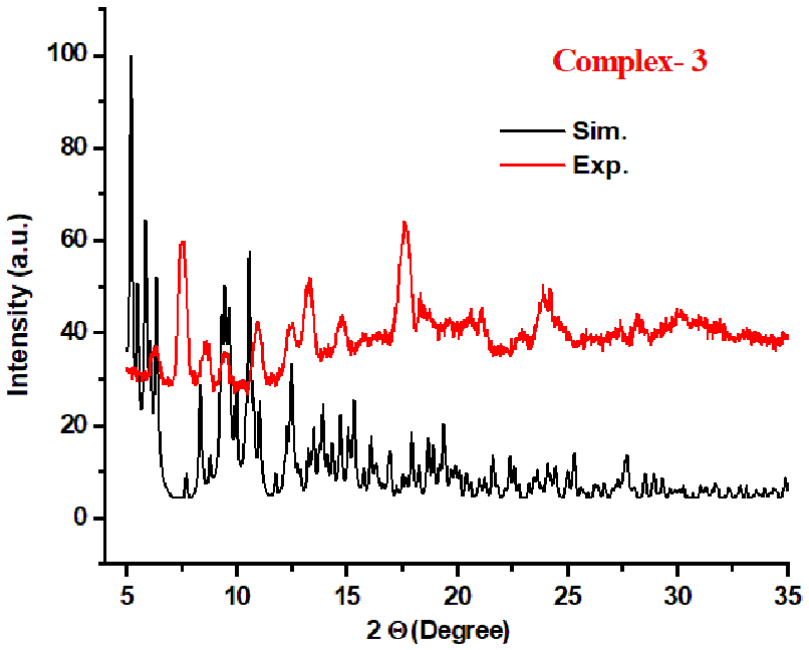

Figure S9: Simulated and experimental PXRD patterns of complex [ClCo(dpgH)$_2$(L$_3$)] **(3)**

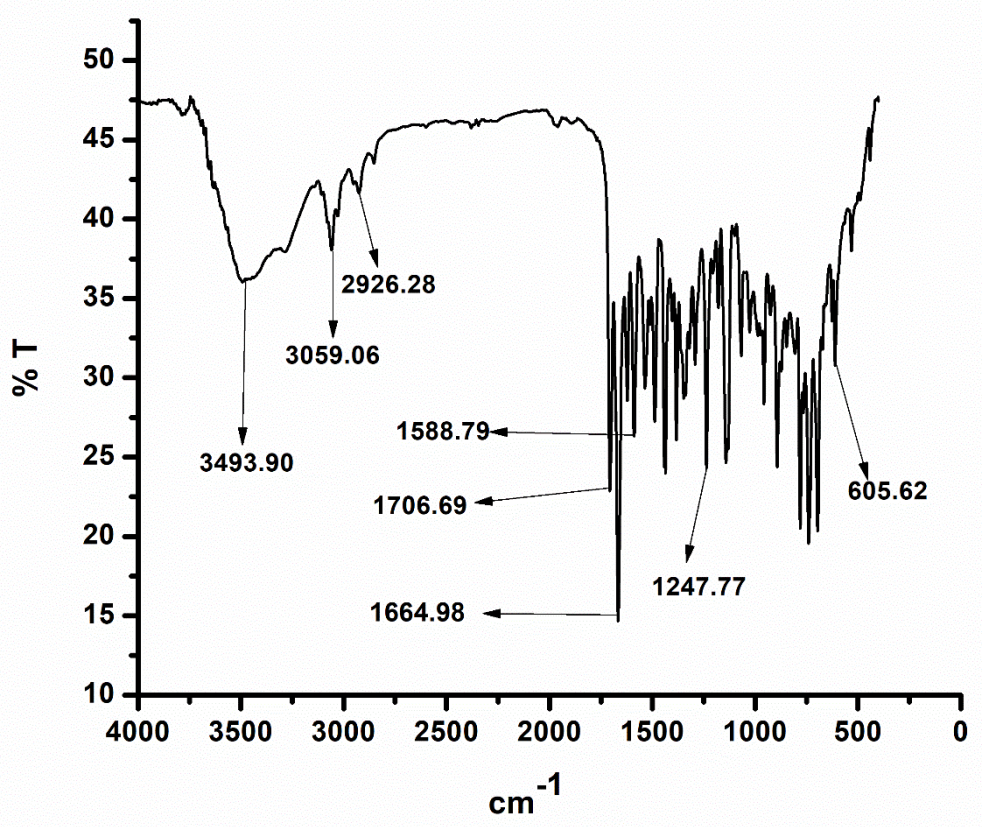

Figure S10: IR Spectrum of Complex [ClCo(dpgH)$_2$(L$_1$)] **(1)**

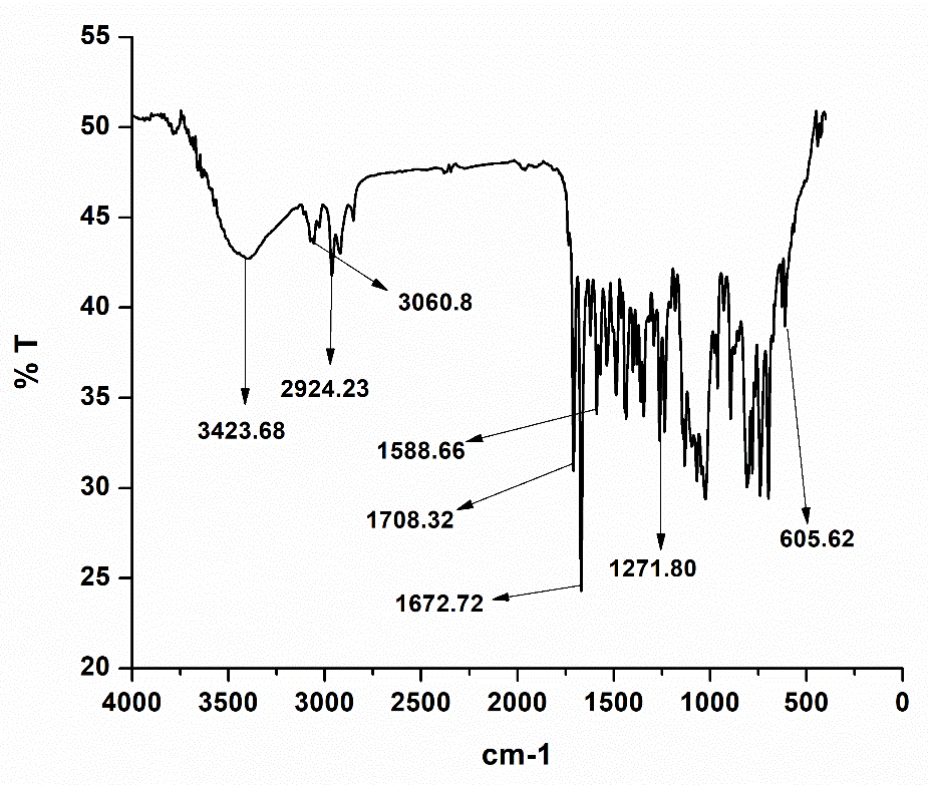

Figure S11: IR Spectrum of Complex $[ClCo(dpgH)_2(L_2)]$ **(2)**

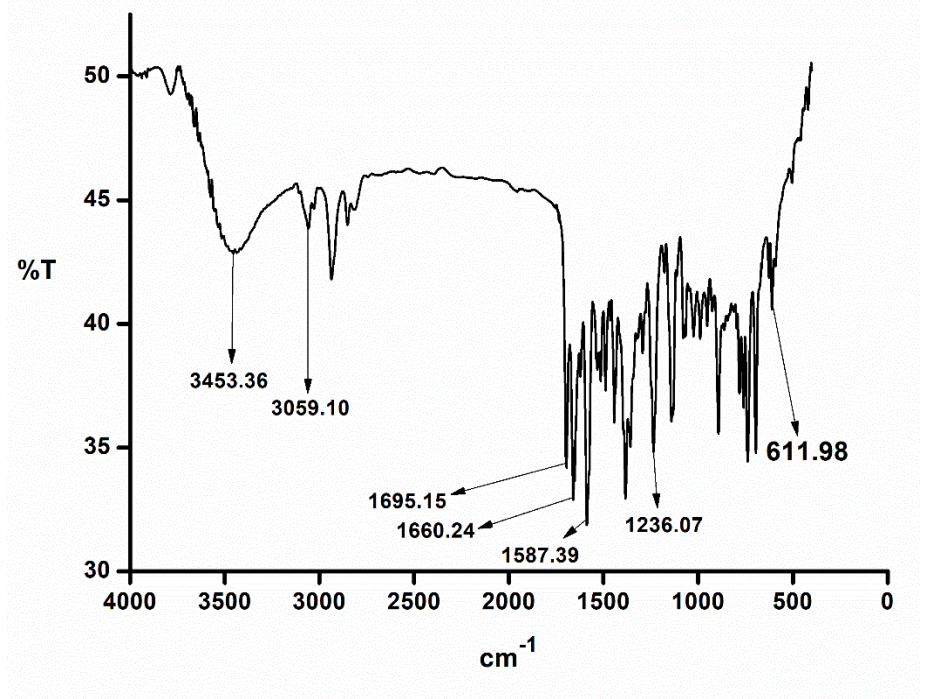

Figure S12: IR Spectrum of Complex $[ClCo(dpgH)_2(L_3)]$ **(3)**

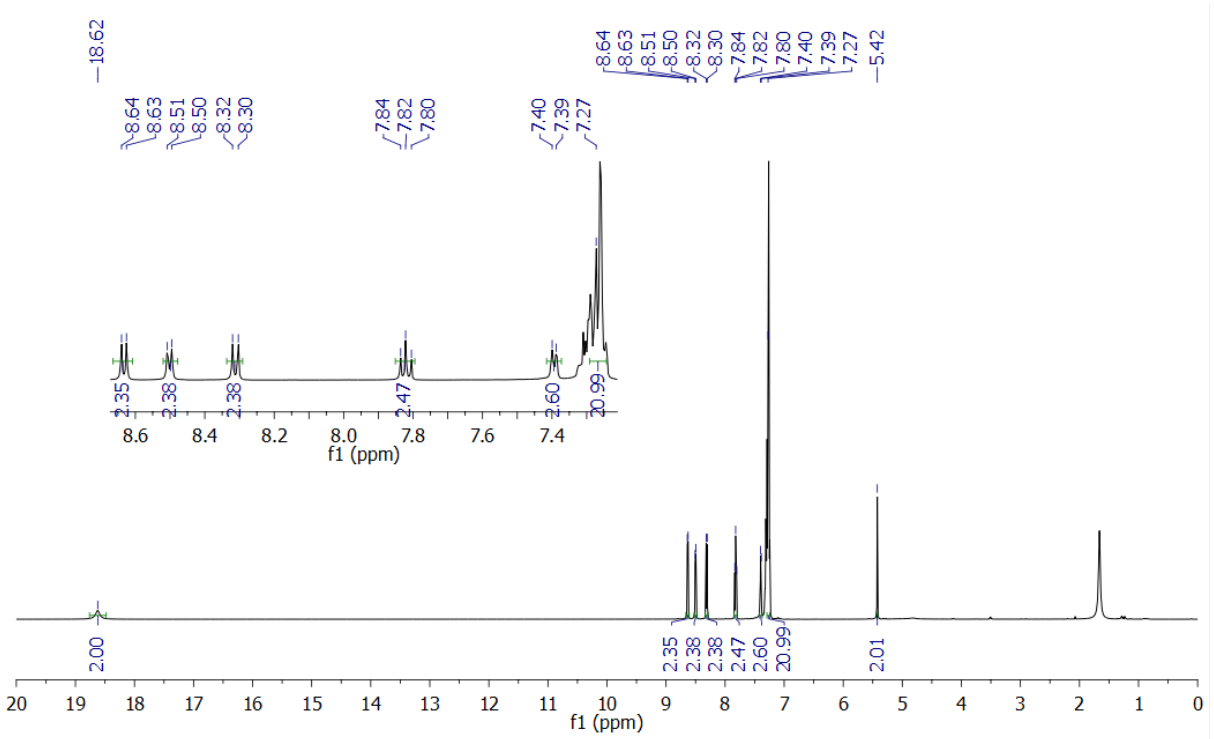

Figure S13: ^{1}H NMR spectrum (500 MHz, $CDCl_3$) of $[ClCo(dpgH)_2(L_1)]$ **(1)**

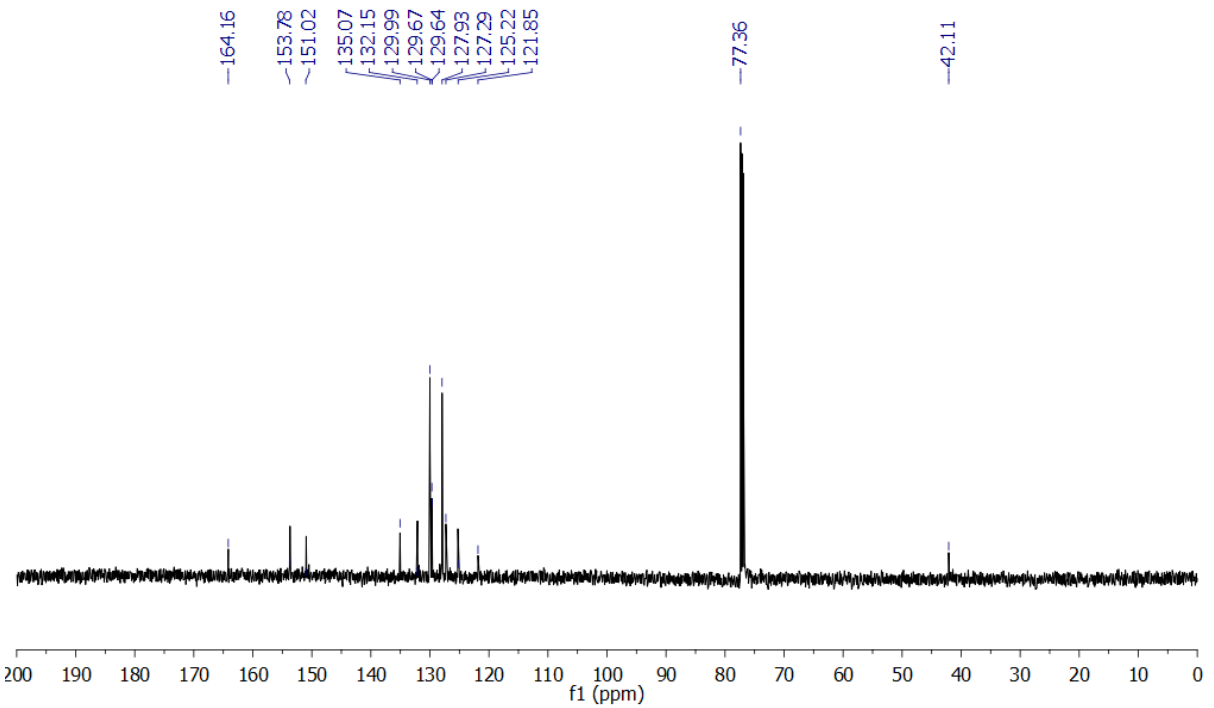

Figure S14: $^{13}C\{^{1}H\}$ NMR spectrum (125 MHz, $CDCl_3$) $[ClCo(dpgH)_2(L_1)]$ **(1)**

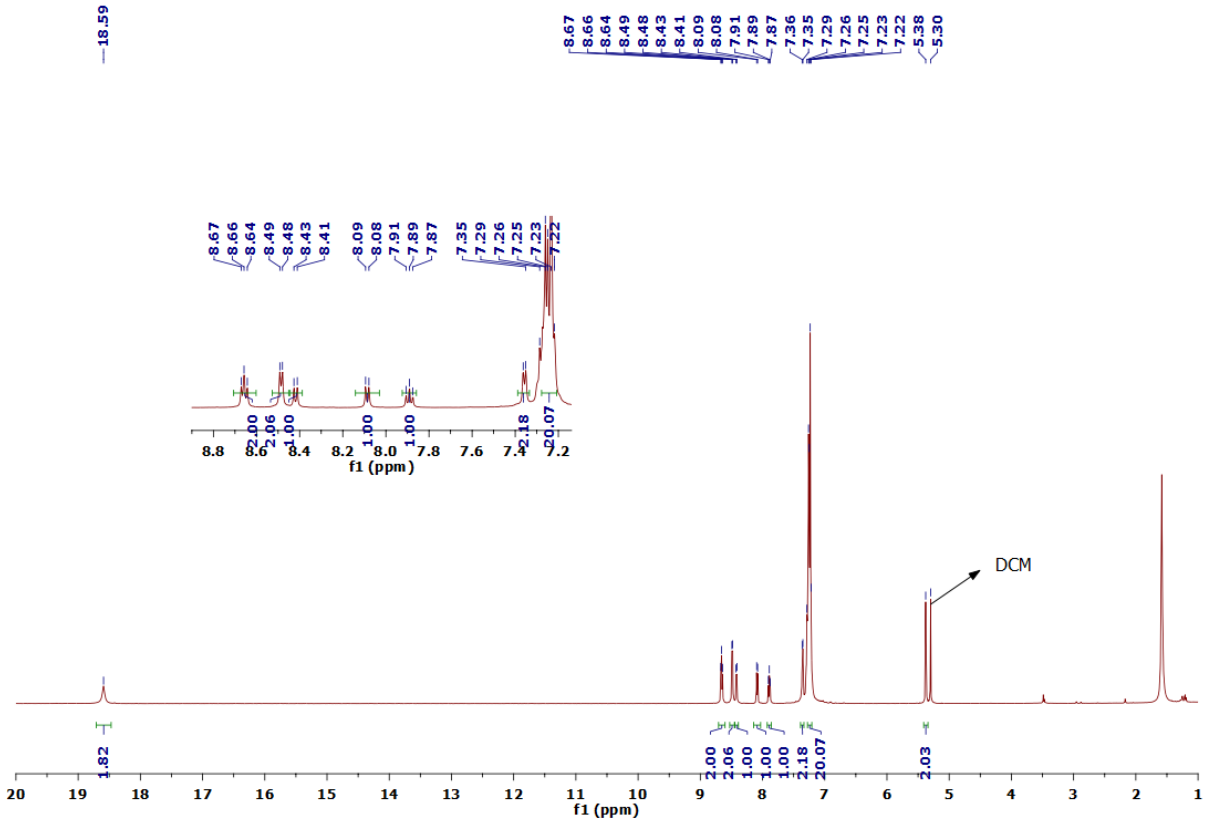

Figure S15: ^{1}H NMR spectrum (500 MHz, $CDCl_3$) of $[ClCo(dpgH)_2(L_2)]$ **(2)**

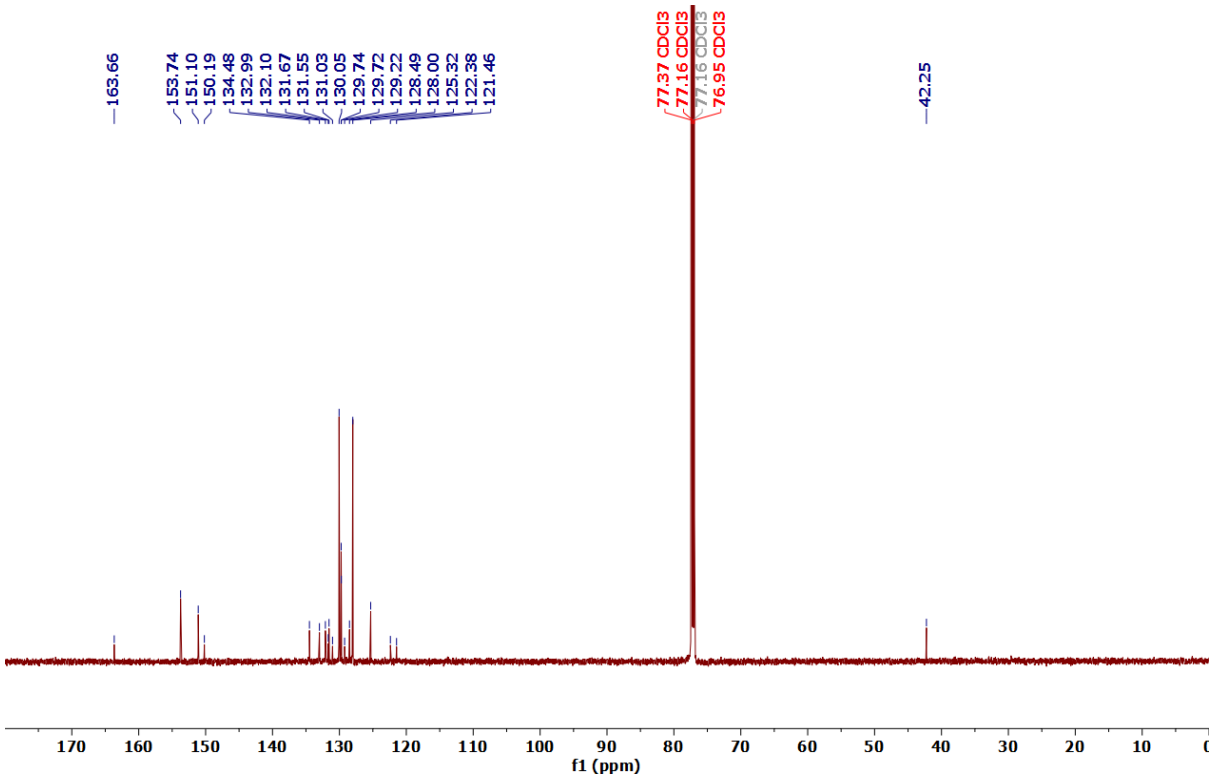

Figure S16: $^{13}C\{^{1}H\}$ NMR (125 MHz, $CDCl_3$) $[ClCo(dpgH)_2(L_2)]$ **(2)**

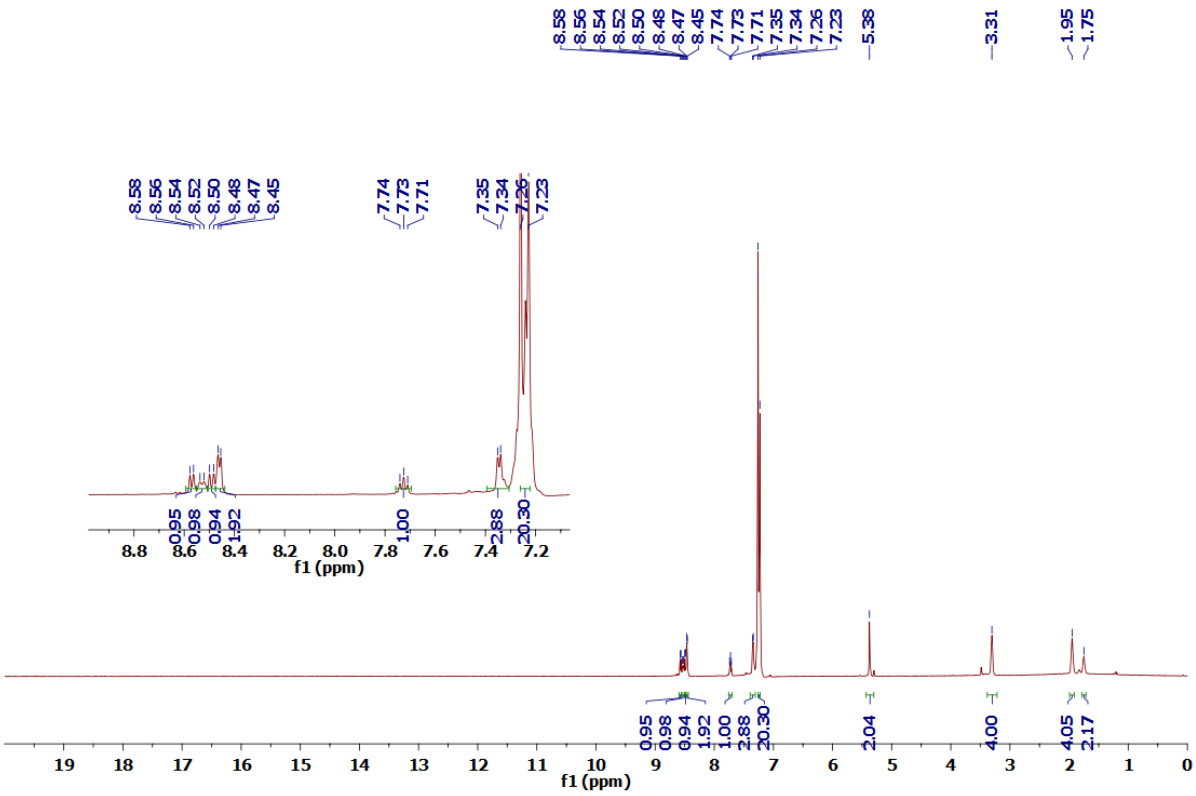

Figure S17: ^{1}H NMR Spectrum (500 MHz, $CDCl_3$) of $[ClCo(dpgH)_2(L_3)]$ **(3)**

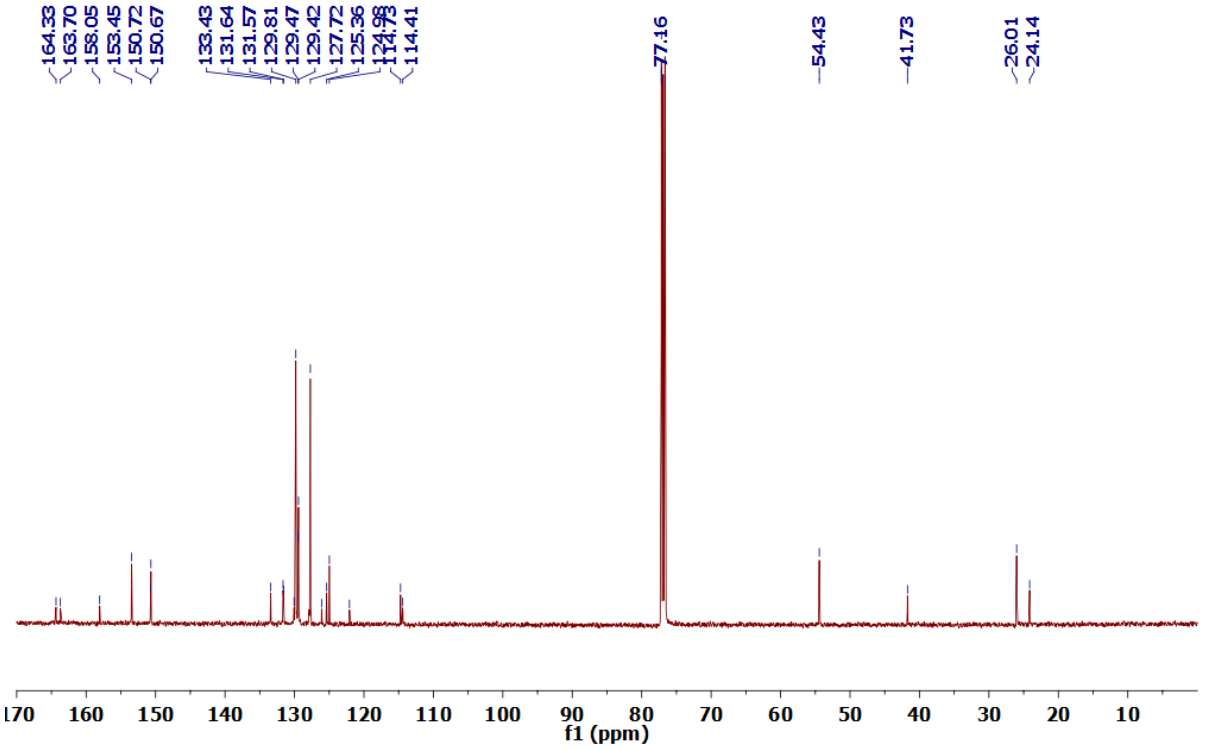

Figure S18: $^{13}C\{^{1}H\}$ NMR spectrum (125 MHz, $CDCl_3$) $[ClCo(dpgH)_2(L_3)]$ **(3)**

Weak non-covalent interactions and supramolecular structures in complexes 1-3

Despite of large number of crystal structures of cobaloximes are reported in literature, very little information is known on weak non-covalent interactions in the solid state leading to novel supramolecular structures.[1-7] Complex **1** reveals various intermolecular non-covalent interactions such as C25–H25···O5, C26-H26···O5 and C4-H4···O6 (Table S1, Figures S19 and S20). A closer inspection on the supramolecular structure of **1** showed dimeric units held together by six types of non-covalent C-H···π interaction i.e. C6-H6···π (C23-C28) having distance 2.875 Å, C13-H13···π (C23-C28) having distance 3.237 Å, C18-H18···π (C9-C14) having distance 3.036 Å, C28-H28···π (C36-C40 and C45) having distance 3.226 Å, C34-H34A···π(C36-C40, C45) having distance 3.382 and C34-H34B···π (C36-C40, C45) having distance 3.337 Å (Table S2, Figures S21-S24). The 1,8-naphthalimide group in complex **1** also sustains a strong **π···π** interaction with a distance 3.558 Å (Figure S21).

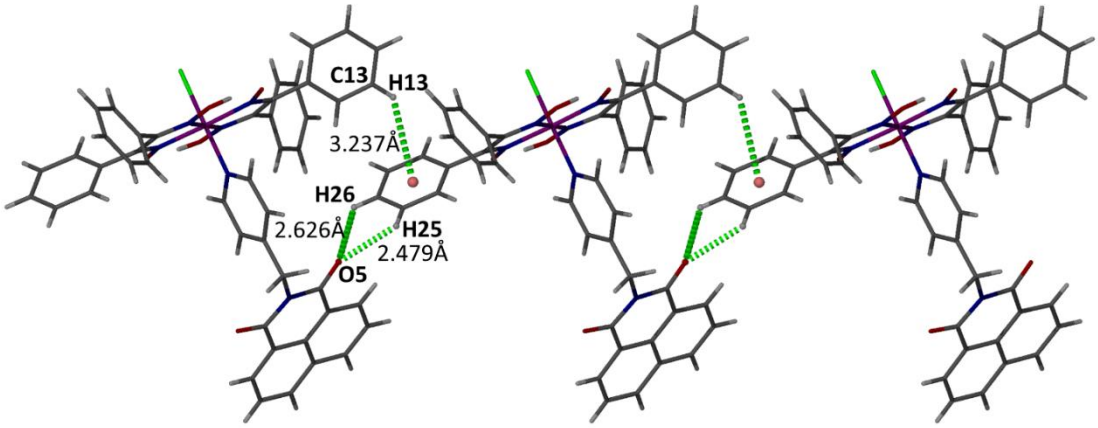

Figure S19: Structure of complex **1** sustained by C–H···**π** (C13-H13…π (C23-C28)) and C–H···O interaction.

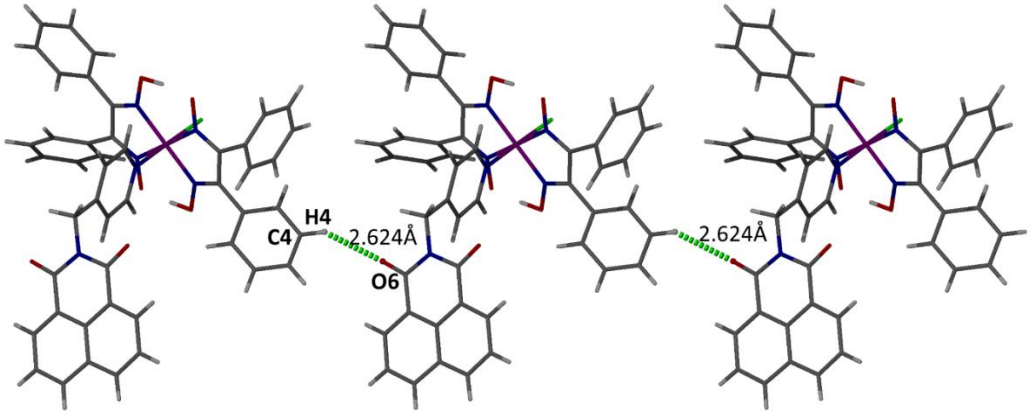

Figure S20: Hydrogen bonded network in complex **1** sustained by C–H···O interaction.

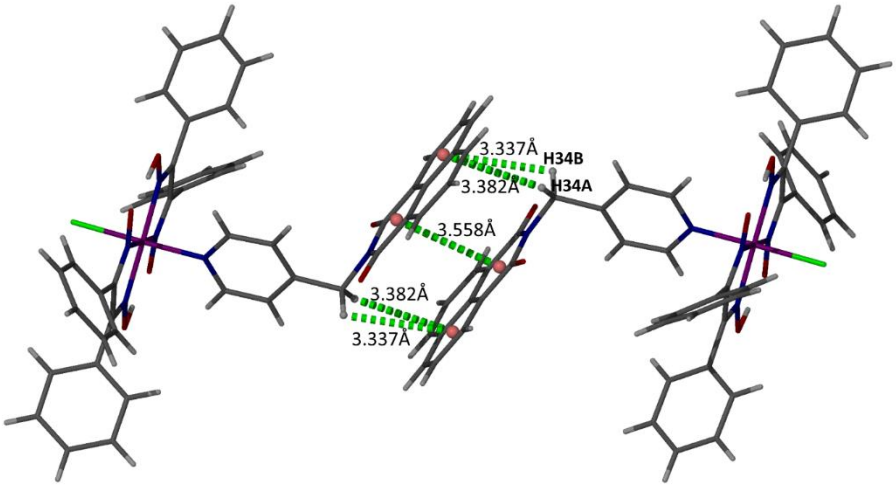

Figure S21: Dimeric unit in complex **1** sustained by C–H···π and π···π interactions.

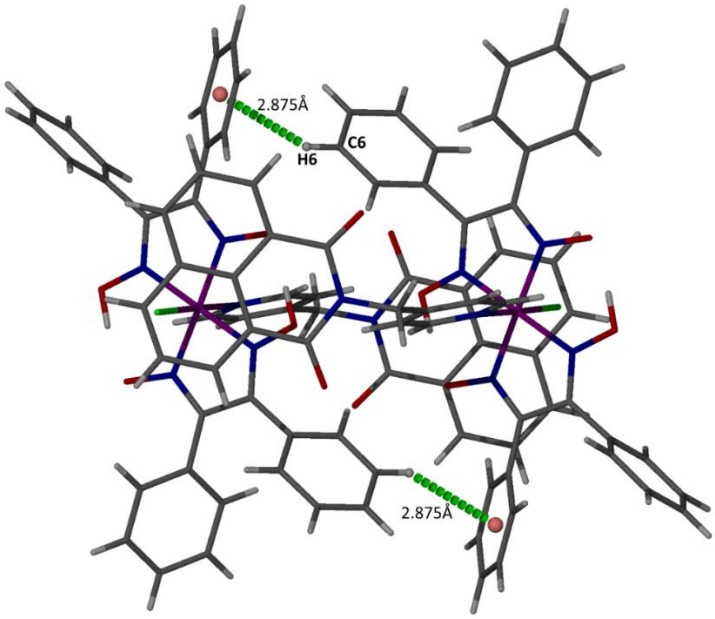

Figure S22: Dimeric unit of complex **1** sustained by C–H···**π** (C6-H6···π (C23-C28)) interaction.

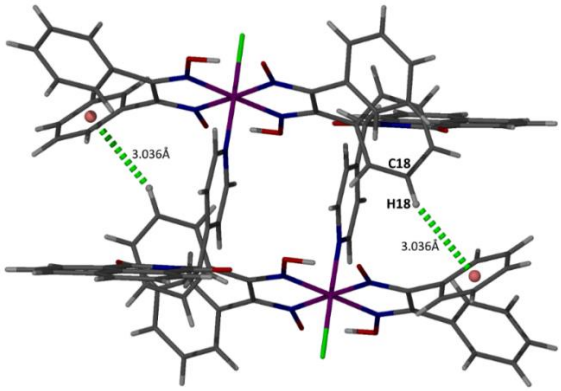

Figure S23: Dimeric unit in complex **1** sustained by C–H···**π** (C18-H18…π (C9-C14)) interaction.

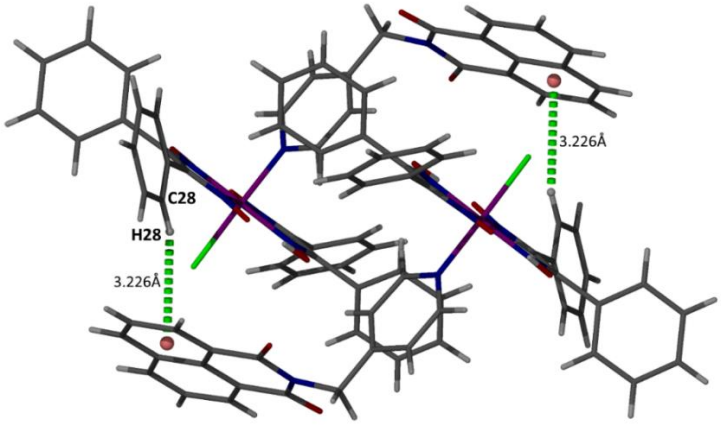

Figure S24: Dimeric unit in complex **1** sustained by C–H···$\boldsymbol{\pi}$ (C28-H28…π (C36-C40 and C45)) interaction.

A deep insight of the supramolecular structure of complex **2** reveals a weaker intermolecular non-covalent interactions like C-H···O (C4-H4···O6A, C25-H25···O5A and C26-H26···O5A), C13-H13··· π(C23-C28) centroid having distance 3.535 Å and C14-H14… π(C23-C28) centroid having distance 3.543 Å that held together a 1D hydrogen bonded polymeric network (Tables S1 and S2, Figures S25-S26). In addition, C-H···π interactions such as C34-H34A···π(centroid of C36A-C41A) and C34-H34B···π(centroid of C36A-C41A) exist, which supports the dimeric unit in the complex (Table S2, Figure S27). Furthermore, in complex **2**, the 1,8-naphthalimide containing bromo group is supported by π···π interaction with the distance of 3.781 Å (Figure S27) similar to complex **1**.

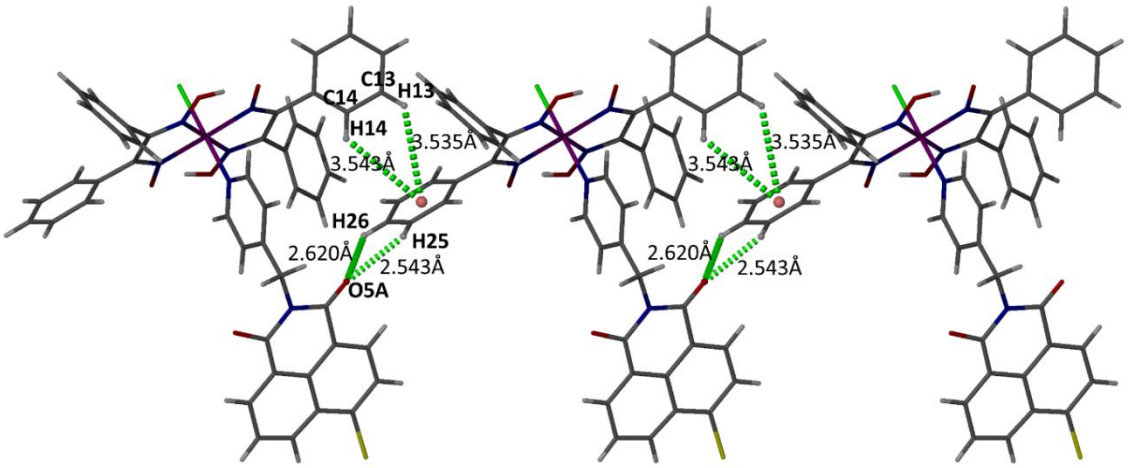

Figure S25: 1D Hydrogen bonded network in complex **2** sustained by C–H···O and C-H···$\boldsymbol{\pi}$ interactions (only the major disordered fraction is kept for clarity).

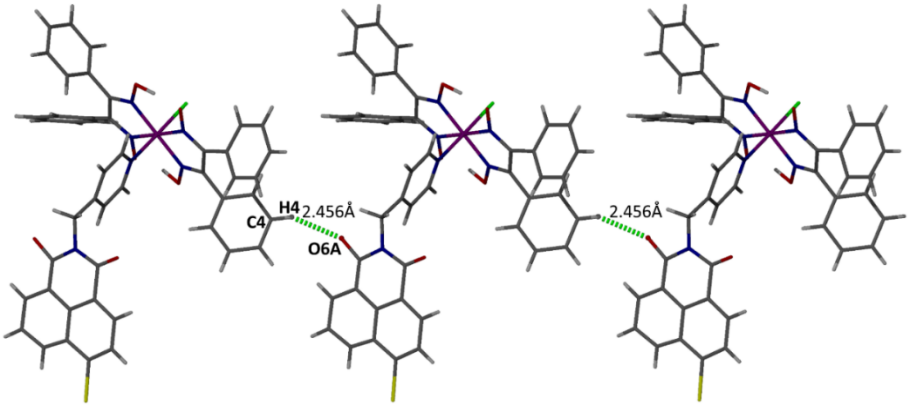

Figure S26: Hydrogen bonded polymeric network of complex **2** sustained by C–H···O interactions (only the major disordered fraction is kept for clarity).

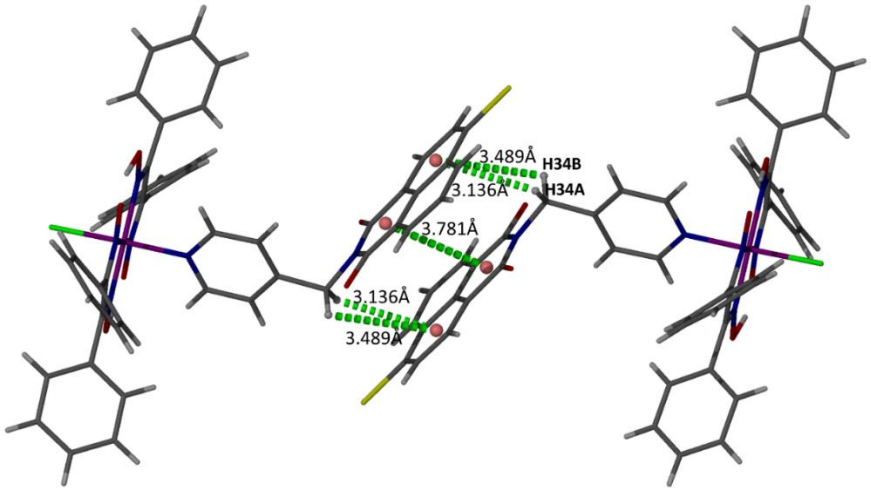

Figure S27: Complex **2** where naphthalimide units are sustained by C–H···π and π···π interactions.

Similar to complexes **1** and **2**, closer examination of the supramolecular structure of complex **3** reveals a weaker intermolecular non-covalent interaction such as C83-H83···O4 and C32-H32···O8 with distance of 2.527 Å and 2.461 Å (Table S1 and Figure S28). Additionally, C-H···π intermolecular interactions such as C27-H27···π(C74-C79) centroid, C64-H64···π(C9-C14) centroid), C85-H85A···π(CC91-C96) and C85-H85B···π(C87-C91, C96) support the two nearby cobaloxime units (Table S2, Figure S29). Furthermore, in complex **3**, the 1,8-naphthalimide containing piperidine group showed π···π interactions with distances of 3.557 Å, 3.605 Å, 3.618 Å and 3.712 Å (Figure S30). Complex **3** also exhibited a C–H···Cl non-bonding interaction with a distance 2.885 Å leading to the 1D supramolecular structures (Table S1 and Figure S31).

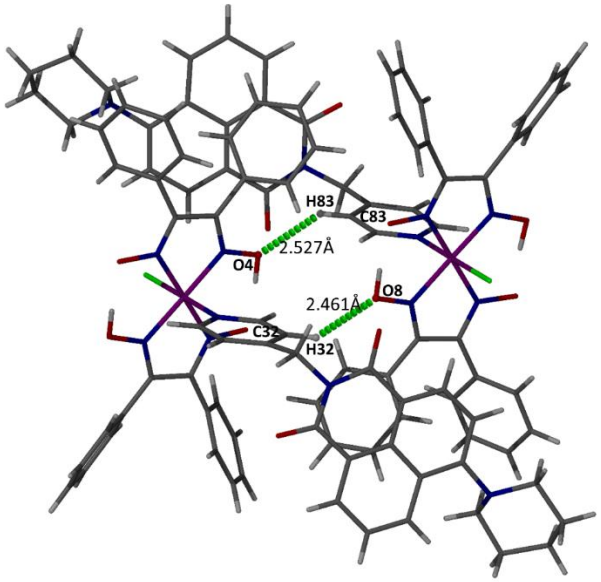

Figure S28: Dimeric unit in complex **3** sustained by C–H···O interaction.

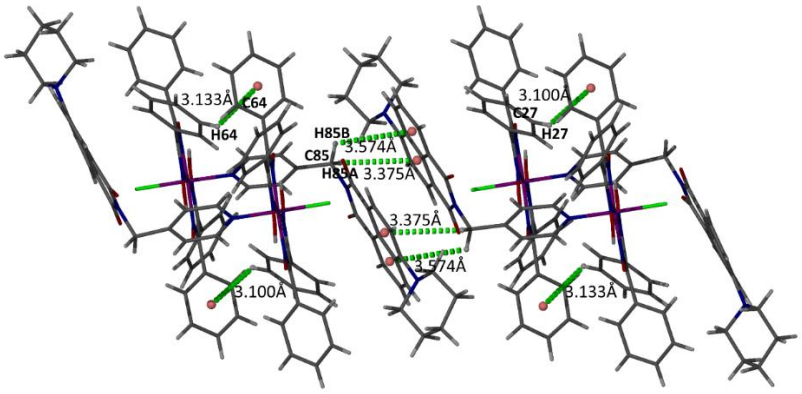

Figure S29: Complex **3** consisting of several C–H···π interactions.

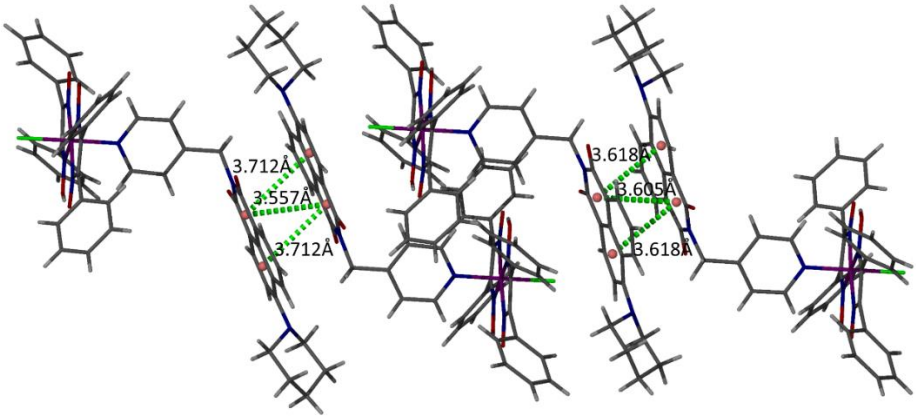

Figure S30: Structure of complex **3** sustained by multiple π···π interactions through naphthalamide unit.

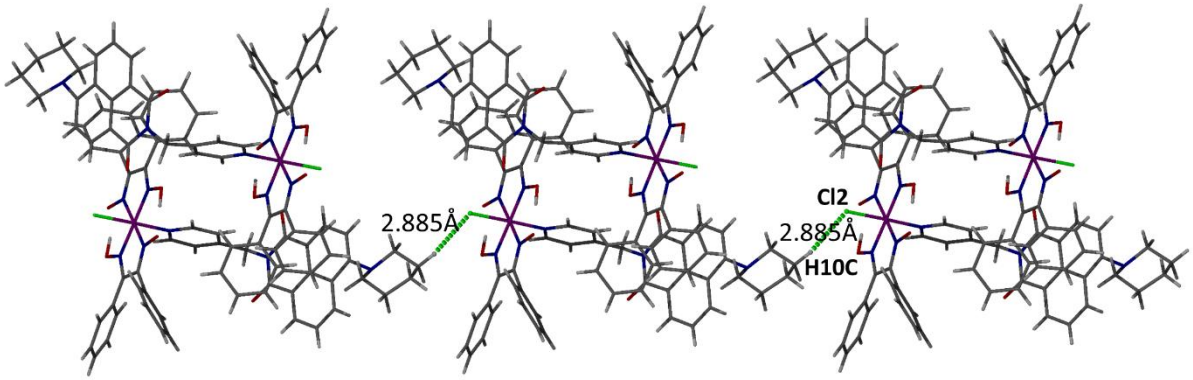

Figure S31: Hydrogen bonded network in complex **3** sustained by C–H···Cl interaction.

Table S1: List of non-bonding intermolecular interactions of complex **1**-**3**.

Complex	D-H···A	D-H (Å)	H···A (Å)	D···A (Å)	D-H···A (°)
1	C4-H4···O6	0.95	2.62	3.39	138.49
	C25-H25···O5	0.95	2.47	3.13	125.56
	C26-H26···O5	0.95	2.62	3.19	119.19
2	C4-H4···O6A	0.95	2.45	3.28	146.38
	C25-H25···O5A	0.95	2.54	3.17	124.40
	C26-H26···O5A	0.95	2.62	3.21	120.90
3	C32-H32·····O8	0.95	2.46	3.23	139.11
	C83-H83·····O4	0.95	2.53	3.30	139.29
	C-H···Cl	**C-H (Å)**	**H···Cl (Å)**	**C···Cl (Å)**	**C-H···Cl (°)**
	C101-H10C·····Cl2	0.99	2.88	3.83	160.32

Table S2: List of non-bonding intermolecular C-H···π interactions of complex **1** - **3**.

Complex	C–H···π	distance C–H···π (Å)
1	C6-H6···π(C23-C28)	2.875
	C13-H13···π(C24-C28)	3.237
	C18-H18···π(C9-C14)	3.036
	C28-H28···π(C36-C40, C45)	3.226
	C34-H34A···π(C36-C40, C45)	3.382
	C34-H34B···π(C36-C40, C45)	3.337
2	C13-H13···π(C23-C28)	3.535
	C14-H14···π(C23-C28)	3.543
	C34-H34A···π(C36A-C41A)	3.136
	C34-H34B···π(C36A-C41A)	3.489
3	C27-H27···π(C74-C79)	3.100
	C64-H64···π(C9-C14)	3.133
	C85-H85A···π(C91-C96)	3.375
	C85-H85B···π(C87-C91, C96)	3.574

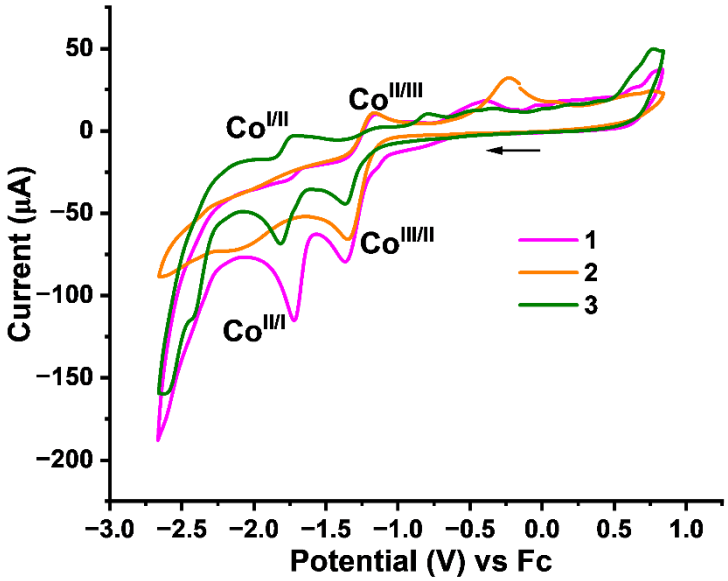

Figure S32. Cyclic voltammograms (CVs) of 1 mM of complexes **1** (purple), **2** (orange), **3** (green) in solution containing 0.1 M $TBAPF_6$ in acetonitrile at 100 mV/s scan rate.

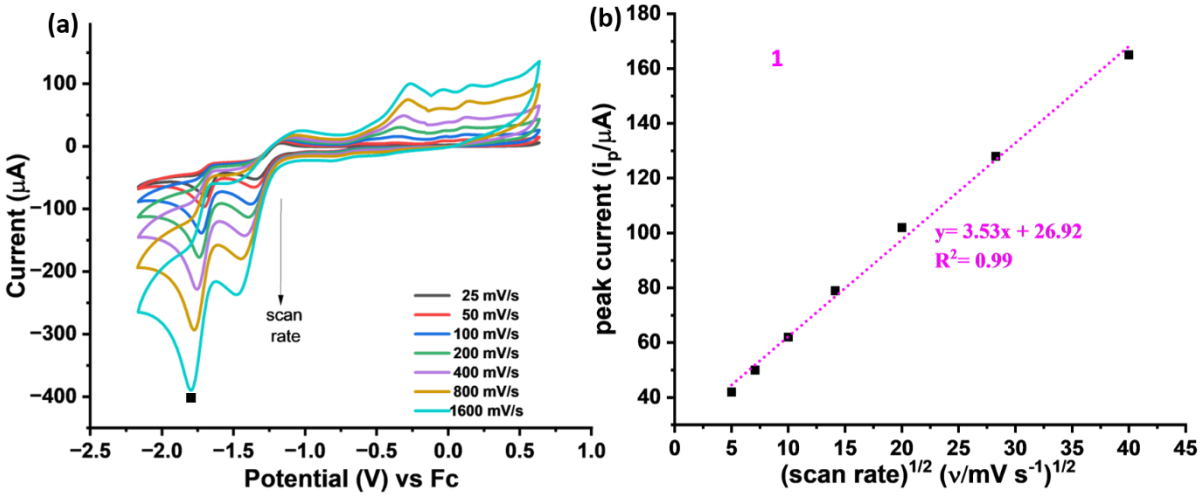

Figure S33: (a) Scan rate variation from 25 mV/s to 1600 mV/s on cyclic voltammogram of 1 mM complex **1** in CH_3CN containing 0.1 M $TBAPF_6$. (b) shows the variation of peak current with the square root of scan rate for complex **1**.

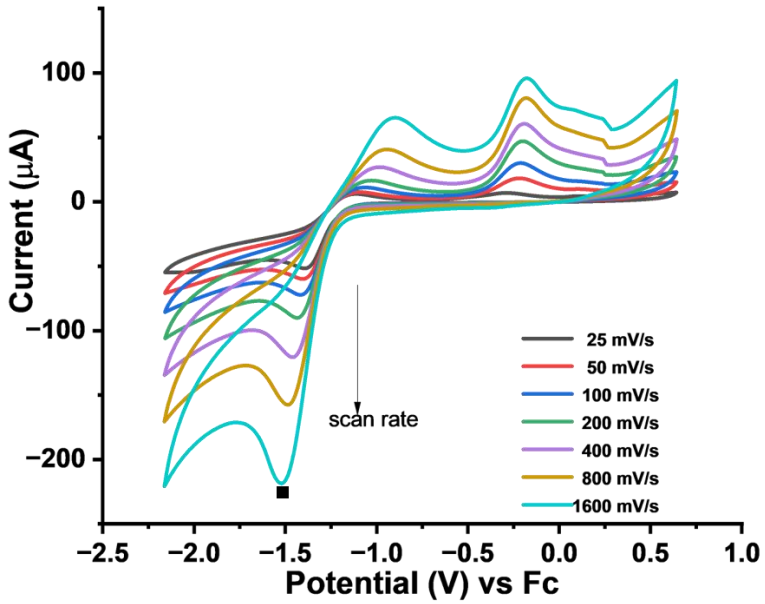

Figure S34: Scan rate variation from 25 mV/s to 1600 mV/s on cyclic voltammogram of 1 mM complex **2** in CH_3CN containing 0.1 M $TBAPF_6$.

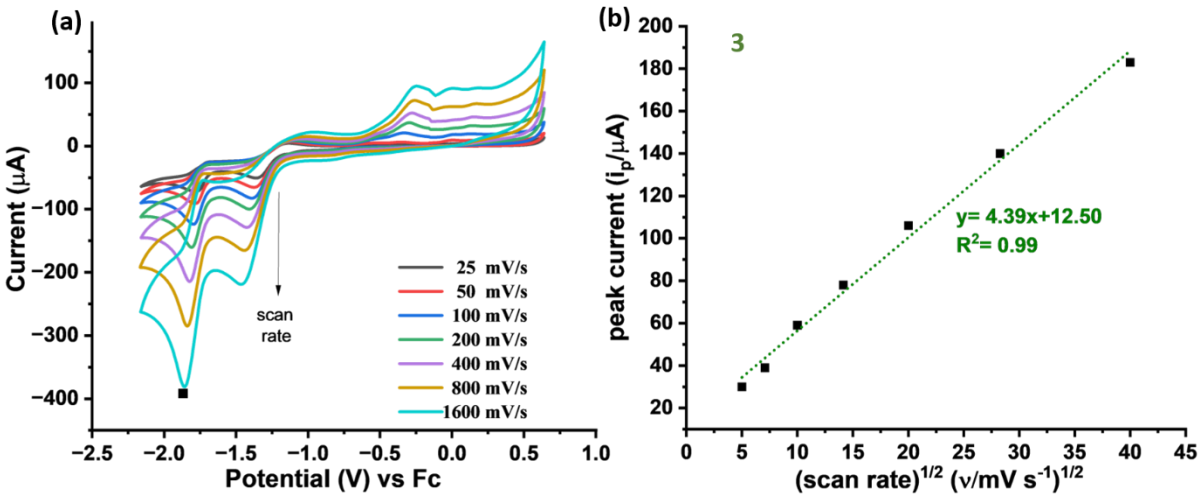

Figure S35: (a) Scan rate variation from 25 mV/s to 1600 mV/s on cyclic voltammogram of 1 mM complex **3** in CH_3CN containing 0.1 M $TBAPF_6$. (b) shows the variation of peak current with the square root of scan rate for complex **3**.

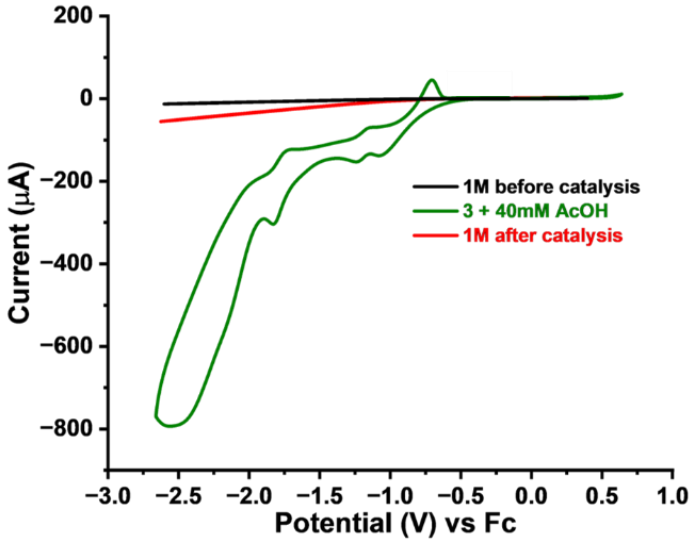

Figure S36: Rinse test for complex **3** (green) in presence of 40 mM AcOH. Black line corresponds to 1M AcOH solution before the catalytic experiment the red line is after the catalysis experiment in 1M AcOH solution at 100 mV/s scan rate vs $Fc^{+/0}$.

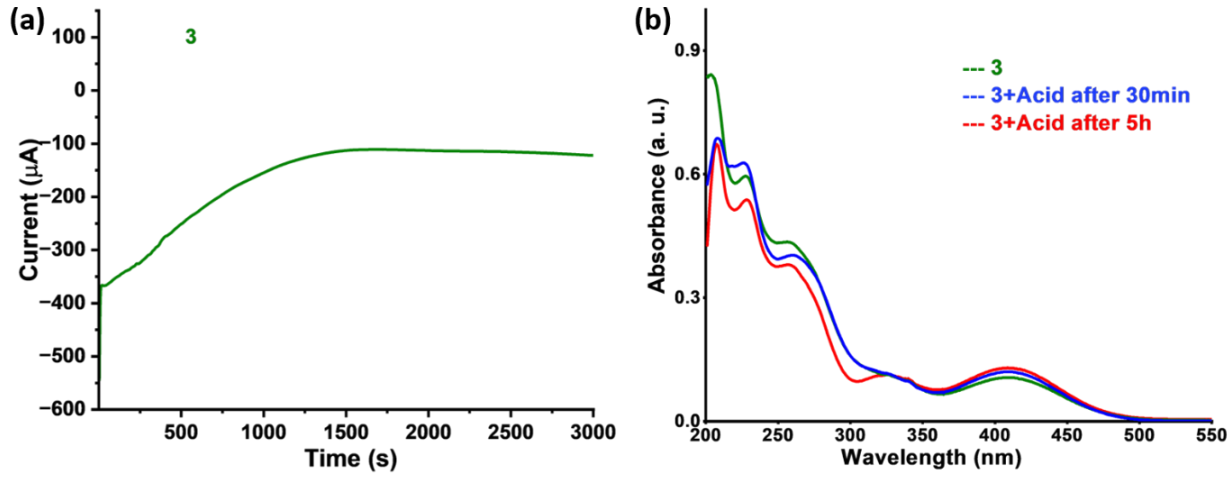

Figure S37: Plot (a) shows the current accumulation over time in the CPE experiment conducted at -2.3 V vs $Fc^{+/0}$ for 1 mM of complex **3** in acetonitrile with 40 mM AcOH and 0.1 M $TBAPF_6$, and (b) represents the UV-Vis. spectra of complex **3** in acetonitrile at 10^{-5} molar concentration in the presence of 25 equivalents of acetic acid.

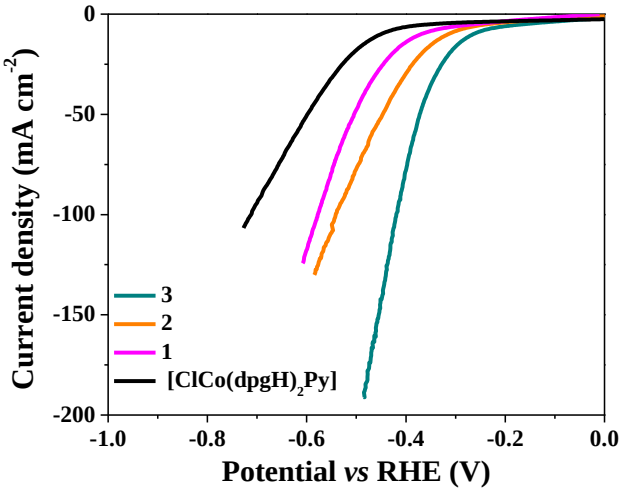

Figure S38: LSV curves for the HER with functionalised CC electrodes i.e. **complex@CC** compared with **[ClCo(dpgH)$_2$py]@CC** showing the best HER activity of **3@CC**.

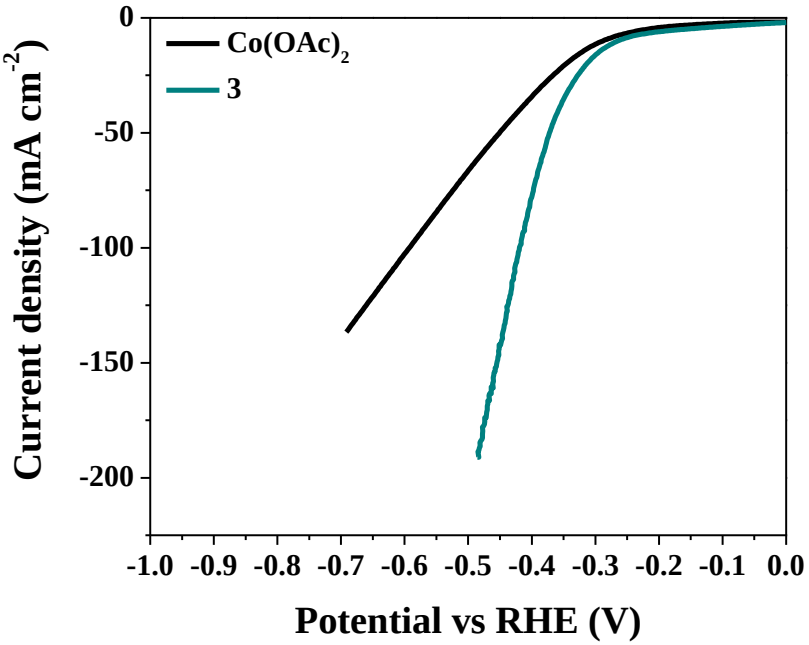

Figure S39: LSV curves for the HER of **3@CC** and **Co(OAc)$_2$@CC** in an alkaline medium.

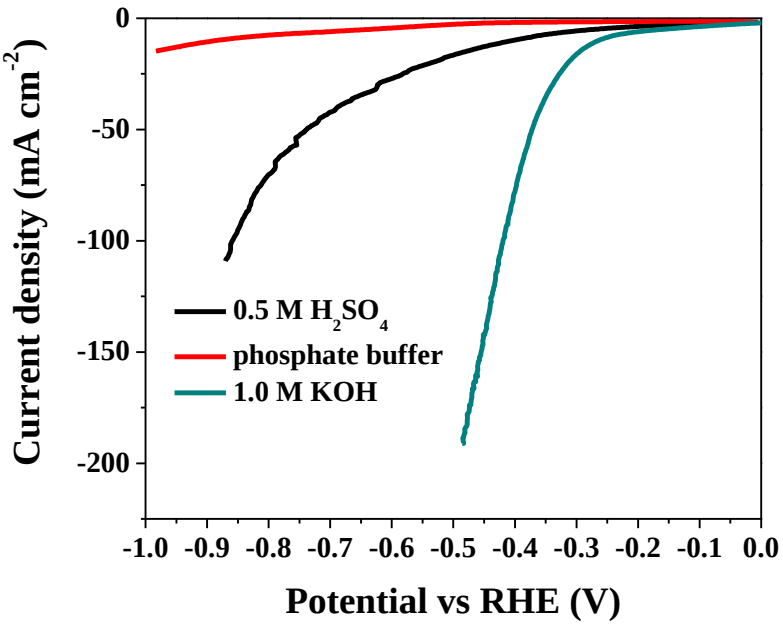

Figure S40: LSV curves for the HER of **3@CC** in acidic, neutral and alkaline medium.

Table S3: Comparison of the HER activities of the synthesized complexes with the literature-reported molecular complexes.

Sr. No.	Electrode	Cobaloxime Catalyst	Overpotential (mV)	Current density (mA cm^{-2})	Electrolyte	References
1	CNT	**Co-a**	590	-1	Acetate(pH 4.5)	*Nat. Chem.* **2013**, *5*, 48-53
2	CNT	**Co-b**	100	-2	Phosphate(pH 6.5)	*Angew. Chem., Int. Ed.* **2016**, *55*, 3952-3957
3	CNT	**Co-c**	100	-2	Phosphate (pH 6.5)	*Angew. Chem., Int. Ed.* **2016**, *55*, 3952-3957
4	Carbon cloth	**Co-d**	200	-4	acetate (pH 4.5)	*Chem. Commun*. **2015**, 51, 11508-11511
5	Carbon Cloth	**1**	375	-10	1.0 M aqueous KOH solution (pH = 13.8)	**This work**
6	Carbon Cloth	**2**	315	-10	1.0 M aqueous KOH solution (pH = 13.8)	**This work**
7	Carbon Cloth	**3**	262	-10	1.0 M aqueous KOH solution (pH = 13.8)	**This work**

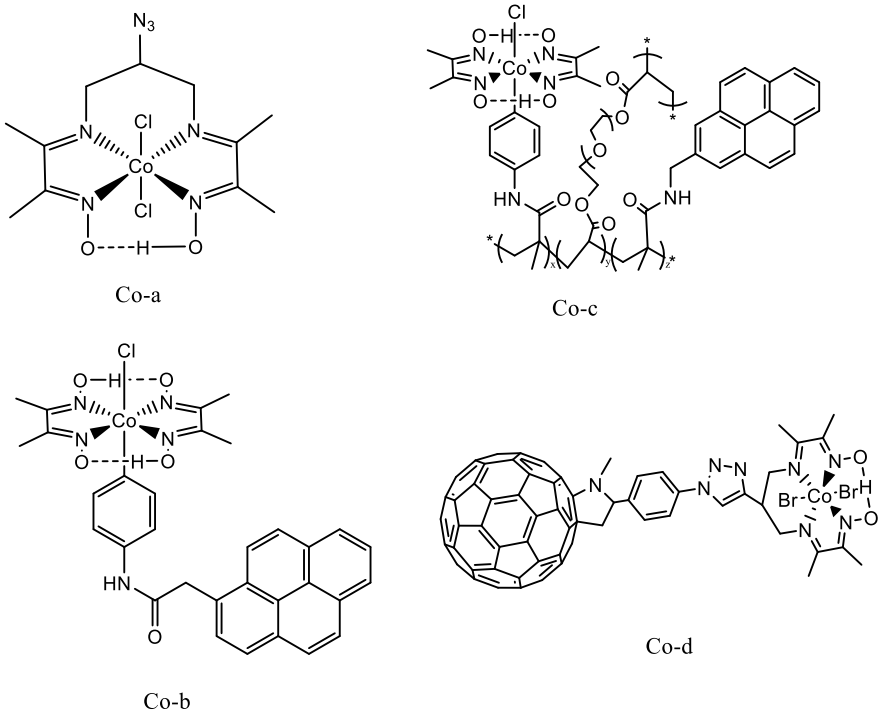

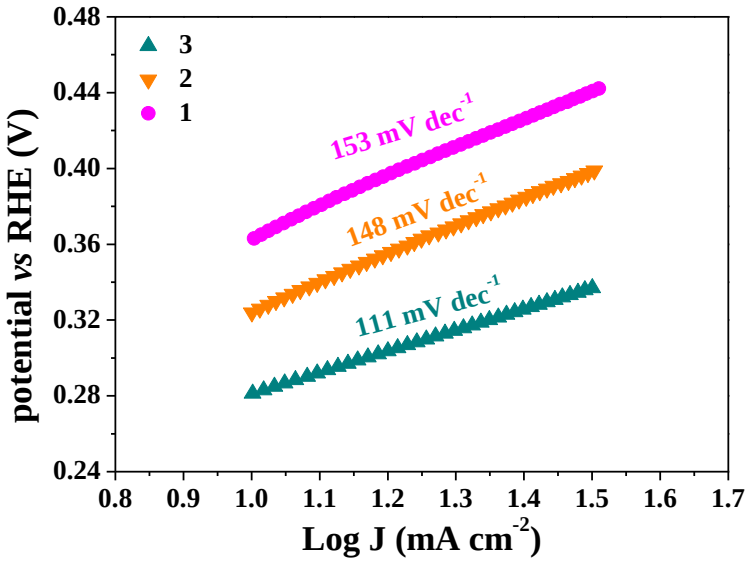

Figure S41: Tafel plots of the **complex@CC** for HER in 1.0 M KOH solution showing the lowest Tafel slope for **3@CC**.

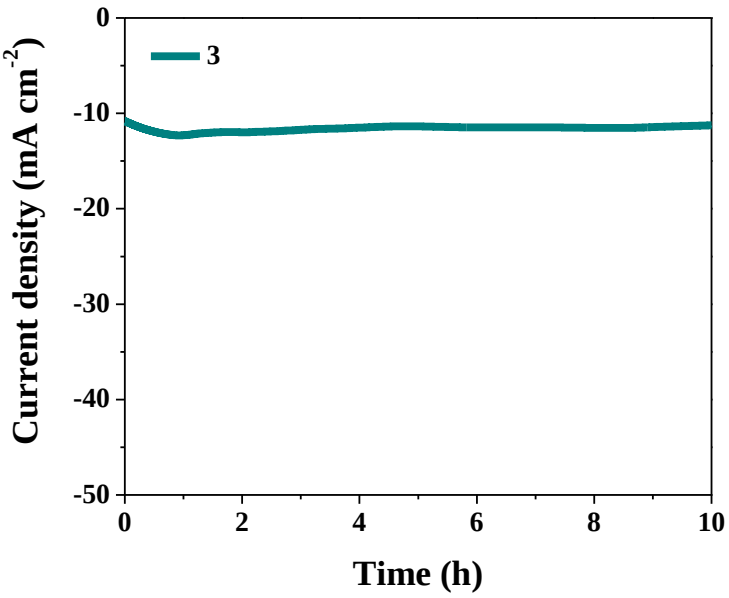

Figure S42: CA stability of **3@CC** showing the enhanced stability for 10 h in 1.0 M KOH solution.

Determination of the faradaic efficiency for HER of catalytic electrode 3@CC

We have utilized the water displacement method to detect the amount of generated hydrogen. The complex-3 was utilized as electrodes with 1 cm^2 surface area. Two-compartment membrane-separated H-cell has been employed to determine the generated hydrogen. We have employed a cathodic current density of -10 mA cm^{-2} for 1800 s.[8-10] In the first step, we calculated the theoretically generated hydrogen gas using the following equation from Faraday's law. [8-10]

$$nH_2\,(theoretical) = \frac{Q}{n \times F} = \frac{I \times t}{n \times F} = \frac{0.01 \times 1800\ s}{2 \times 96485.3\ s\ A\ mol^{-1}} = 0.0932\ mmol$$

Where nH_2 represents the theoretically calculated amount of H_2, Q denotes the amount of applied charge, *n* shows the number of electrons transferred in HER (2 electrons), *F* denotes the Faraday constant (96485.3 s A mol^{-1}), *I* represents the applied current (0.01 A), and *t* is the reaction time (1800 s).

After theoretical calculations, we measured the amount of generated hydrogen in millilitre at the time of chronoamperometric measurements. The generated H_2 gas in millilitre was converted into mmol using Avogadro number (table S4). Further, the experimentally measured and theoretically calculated amount of hydrogen was compared to determine the faradaic efficiency using the following equation:

Table S4: Details of experimentally generated hydrogen gas.

Experimentally generated H_2 gas		
Time (minutes)	**mL (millilitre)**	**mmol**
5	0.338	0.0151
10	0.676	0.0302
15	1.014	0.0453
20	1.352	0.0604
25	1.691	0.0755
30	2.031	0.0907

$$\text{Faradaic efficiency (\%)} = \frac{nH_2\text{ (experimental)}}{nH_2\text{ (Theoretical)}} \times 100 = \frac{0.0907\text{ mmol}}{0.0932\text{ mmol}} \times 100 = 97.3\%$$

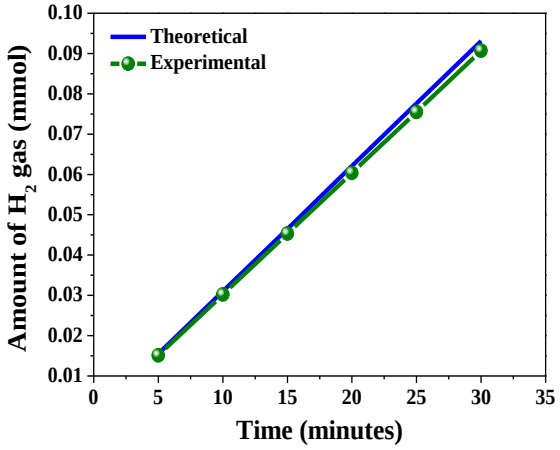

Figure S43: Theoretically and experimentally determined amount of hydrogen to determine the faradaic efficiency of **3@CC**.

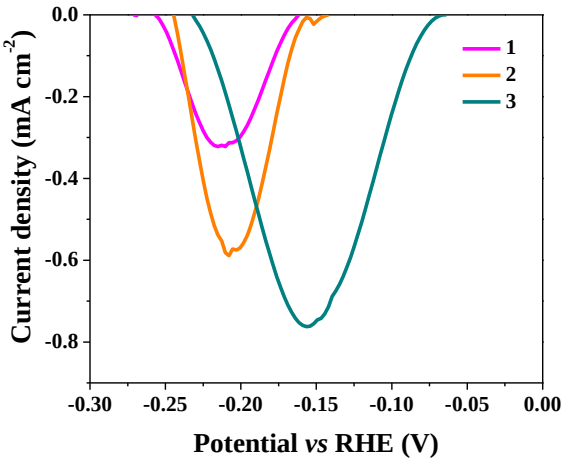

Figure S44: Reduction peaks for **complex@CC** utilized for the integration to calculate the number of active Co-sites (scan rate 20 mV s^{-1}). [11-13]

The number of active sites for catalytic electrodes have been determined by the redox peak integration method. For this purpose, we have carried out CV at the scan rate 20 mV s^{-1} and determined the redox peak. The reduction peak area has been integrated using origin software. The associated charge with the reduction peak of the complexes has been calculated by dividing the reduction peak area with scan rate. As the reduction of Co^{II}/Co^{I} is a one electron transfer process, the associated charge has been divided by the charge of electron to find out the number of surface active sites.[11-13]

Equation S1:

1@CC:

Calculated area associated with the oxidation peak = 0.00155×10^{-3} V A

Hence the associated charge was = 0.00155×10^{-3} V A / 0.02 V s^{-1}

$= 0.0775 \times 10^{-3}$ As

$= 0.0775 \times 10^{-3}$ C

Now, the number of electron transferred was = 0.0775×10^{-3} C / 1.602×10^{-19} C

$= 0.0483 \times 10^{16}$

$= 4.83 \times 10^{14}$

The number of electrons calculated above was the same as the number of the surface active site due to a single electron transfer involving the Co^{3+}/Co^{2+} process.

Hence,

The surface-active site that participated in HER = **4.83×10^{14}**

2@CC:

Calculated area associated with the oxidation peak = 0.00423×10^{-3} V A

Hence the associated charge was = 0.00423×10^{-3} V A / 0.02 V s^{-1}

$= 0.2115 \times 10^{-3}$ As

$= 0.2115 \times 10^{-3}$ C

Now, the number of electron transferred was = 0.2115×10^{-3} C / 1.602×10^{-19} C

$= 0.1320 \times 10^{16}$

$= 13.20 \times 10^{14}$

The surface-active site that participated in HER = **13.20×10^{14}**

3@CC:

Calculated area associated with the oxidation peak = 0.00742×10^{-3} V A

Hence the associated charge was = 0.00742×10^{-3} V A / 0.02 V s^{-1}

$= 0.3710 \times 10^{-3}$ As

$= 0.3710 \times 10^{-3}$ C

Now, the number of electron transferred was = 0.3710×10^{-3} C / 1.602×10^{-19} C

$= 0.2315 \times 10^{16}$

$= 23.15 \times 10^{14}$

The surface-active site that participated in HER = **23.15×10^{14}**

Equation S2:

Calculation of Turn Over Frequency (TOF)[4-6]

$TOF = (j \times N_A) / (2 \times F \times n)$

Where,

j = current density at 262 mV

N_A = Avogadro number

F = Faraday constant

n = number of active Co-sites

As the complex 3 has shown the best HER activity at 262 mV overpotential producing 10 mA cm^{-2} current density, we have calculated the TOF at 262 mV overpotential for all the complexes resulting in the exact comparison of the TOF.

1@CC:

$TOF = [(5.2 \times 10^{-3}) (6.023 \times 10^{23})] / [(96485) (2) (4.83 \times 10^{14})]$

$TOF = 33.6\ s^{-1}$

2@CC:

$TOF = [(6.5 \times 10^{-3}) (6.023 \times 10^{23})] / [(96485) (2) (13.20 \times 10^{14})]$

$TOF = 15.3\ s^{-1}$

3@CC:

$TOF = [(10.0 \times 10^{-3}) (6.023 \times 10^{23})] / [(96485) (2) (23.15 \times 10^{14})]$

$TOF = 13.4\ s^{-1}$

Equation S3:

Calculation of exchange current density *(Catal. Sci. Technol., 2021,11, 6832-6838, J. Phys. Chem. B 1997, 101, 27, 5405–5413)*

$I_0 = I \times R \times T / \eta \times F$

For 1@CC

$I_0 = 5.2 \times 8.314 \times 298.15 / 262 \times 96485 = 5.09 \times 10^{-4}$ mA cm^{-2}

For 2@CC

I_0 = 6.5 × 8.314 × 298.15 / 262 × 96485 = 6.37 × 10^{-4} mA cm^{-2}

For 3@CC

I_0 = 10.0 × 8.314 × 298.15 / 262 × 96485 = 9.80 × 10^{-4} mA cm^{-2}

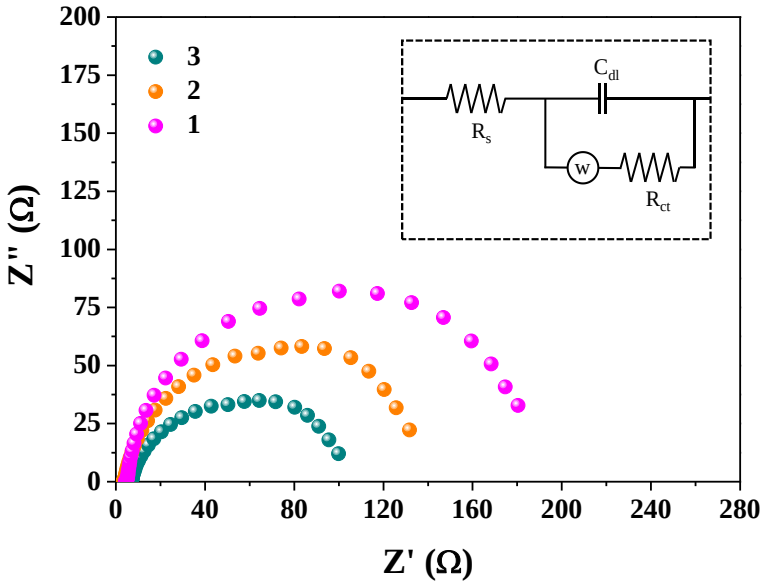

Figure S45: EIS plots for **complex@CC** showing the lowest R_{ct} value for **3@CC**.

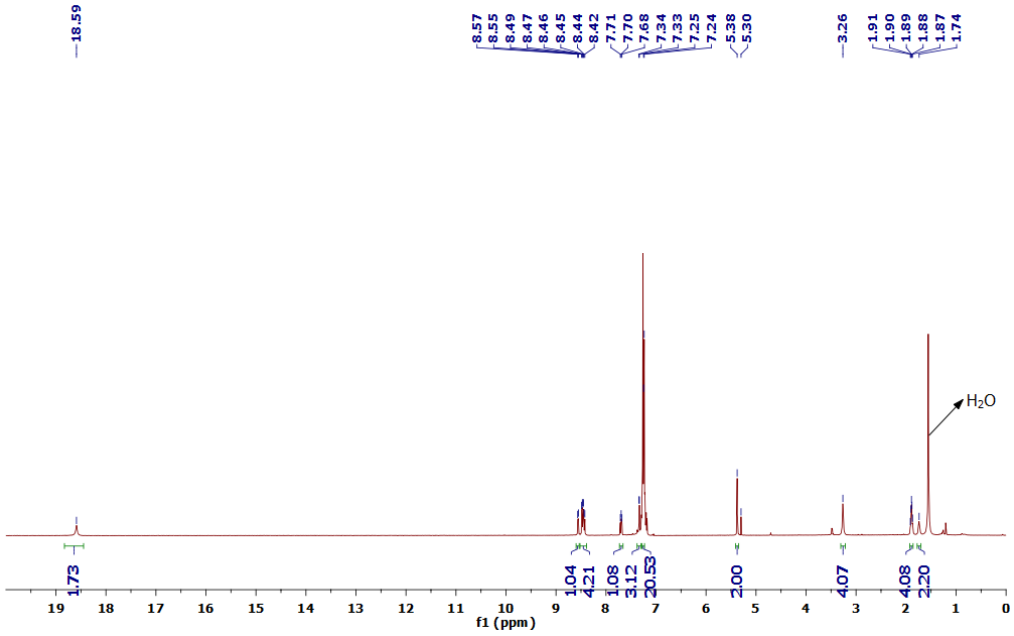

Figure S46: ^{1}H NMR Spectrum (500 MHz, $CDCl_3$) of [$ClCo(dpgH)_2(L_3)$] **(3)** after catalysis.

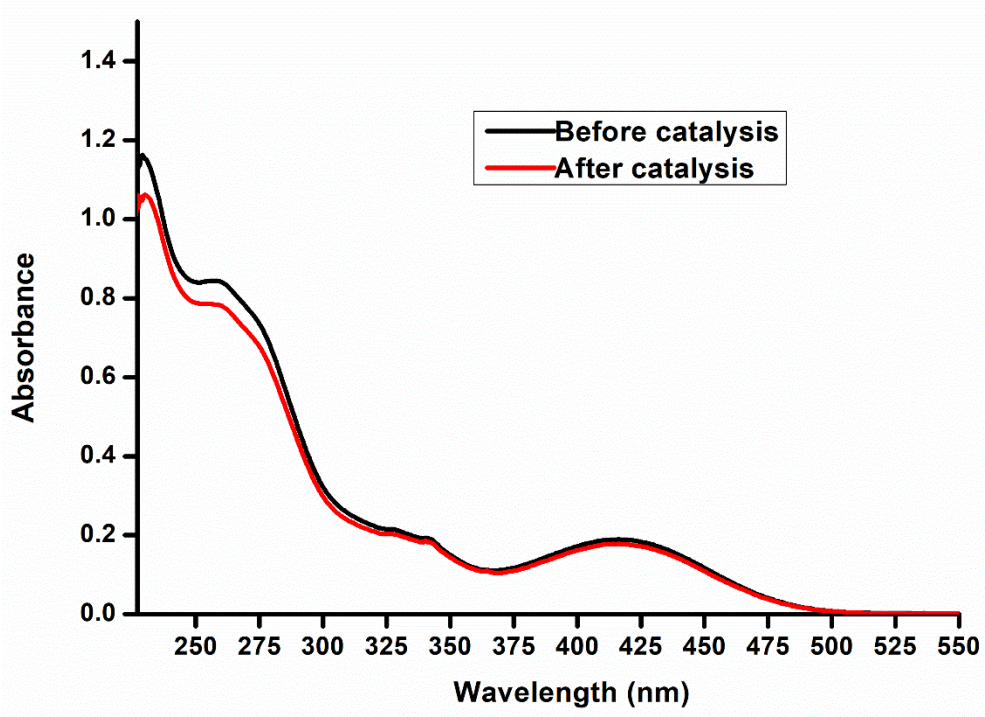

Figure S47: UV-Vis spectra of complex **3 (**After and before the catalysis) in CH_2Cl_2 solution at 10^{-5} molar concentration.

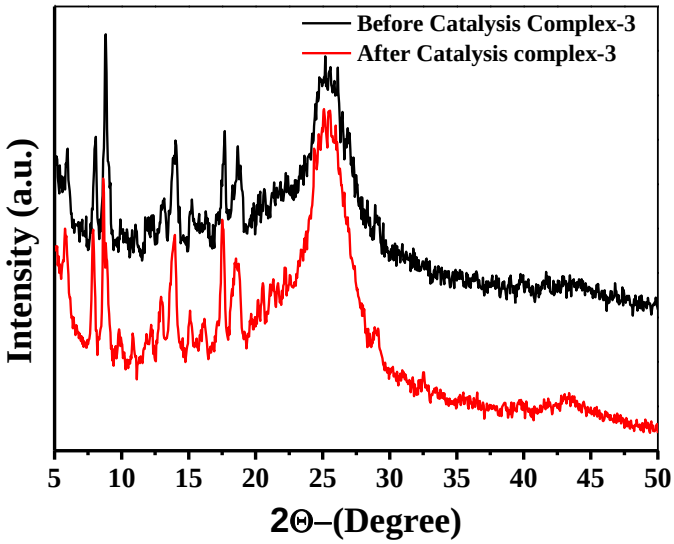

Figure S48: PXRD patterns of **3@CC** before the HER catalysis and after the HER catalysis indicating the existence of molecular entity after catalysis.

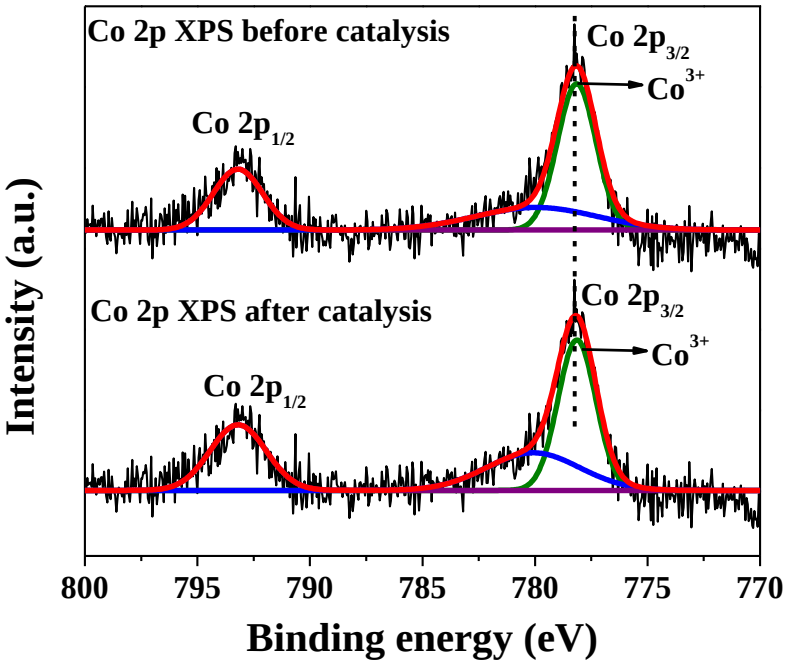

Figure S49: Co 2p XPS spectrum of **3@CC** before and after the HER catalysis.

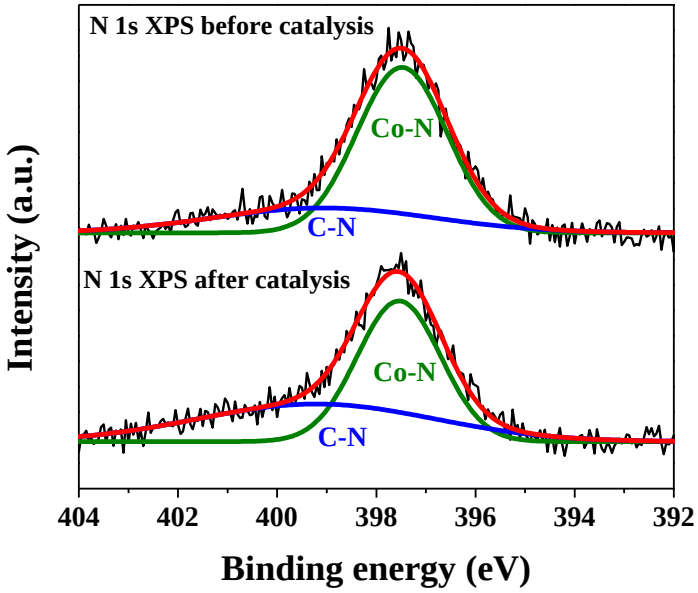

Figure S50: N 1s XPS spectrum of **3@CC** before and after the HER catalysis.

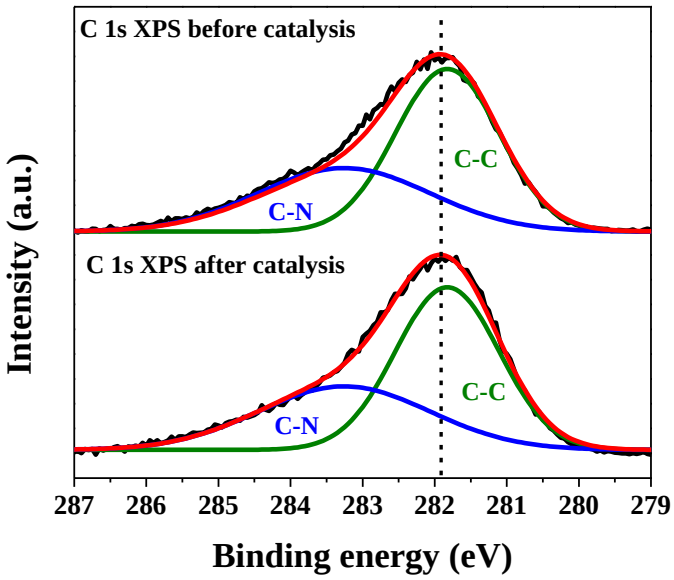

Figure S51: C 1s XPS spectrum of **3@CC** before and after the HER catalysis.

References:

1. K. Kumar and B. D. Gupta, *J. Organomet. Chem.*, 2011, **696**, 2280-2286.
2. K. Kumar and B. D. Gupta, *J. Organomet. Chem.*, 2011, **696**, 3785-3791.
3. B. Gupta, R. Yamuna and D. Mandal, *Organometallics*, 2006, **25**, 706-714.
4. B. Gupta, V. Singh, R. Yamuna, T. Barclay and W. Cordes, *Organometallics*, 2003, **22**, 2670-2678.
5. B. Gupta, V. Vijaikanth and V. Singh, *Organometallics*, 2004, **23**, 2069-2079.
6. Z. Xin, H. Deyan, L. Yizhi and C. Huilan, *Inorg. Chim. Acta*, 2006, **359**, 1121-1128.
7. X. Zhang, Y. Li, Y. Mei and H. Chen, *J. Organomet. Chem.*, 2006, **691**, 659-666.
8. J. Jia, L. C. Seitz, J. D. Benck, Y. Huo, Y. Chen, J. W. D. Ng, T. Bilir, J. S. Harris and T. F. Jaramillo, *Nat. Commun.*, 2016, **7**, 1-6.
9. A. Paracchino, V. Laporte, K. Sivula, M. Grätzel and E. Thimsen, *Nat. Mater.*, 2011, **10**, 456-461.
10. I. M. Mosa, S. Biswas, A. M. El-Sawy, V. Botu, C. Guild, W. Song, R. Ramprasad, J. F. Rusling and S. L. Suib, *J. Mater. Chem. A*, 2016, **4**, 620-631.

11. S. Anantharaj, S. Ede, K. Karthick, S. S. Sankar, K. Sangeetha, P. Karthik and S. Kundu, *Energy & Environ. Sci.*, 2018, **11**, 744-771.
12. B. Singh and A. Indra, *Dalton Trans.*, 2021, **50**, 2359-2363.
13. B. Singh, Y.-C. Huang, A. Priyadarsini, P. Mannu, S. Dey, G. K. Lahiri, B. S. Mallik, C.-L. Dong and A. Indra, *J. Mater. Chem. A*, 2023, **11**, 15906-15914.